CANCER GENOMICS & PROTEOMICS *18*: 385-405 (2021)
doi:10.21873/cgp.20267

Metabolic Response to the Mitochondrial Toxin 1-Methyl-4-phenylpyridinium (MPP+) in LDH-A/B Double-knockout LS174T Colon Cancer Cells

NZINGA MACK, ELIZABETH MAZZIO, RAMESH BADISA and KARAM F.A. SOLIMAN

Pharmaceutical Sciences Division, College of Pharmacy & Pharmaceutical Sciences, Institute of Public Health, Florida A&M University, Tallahassee, FL, U.S.A.

Abstract. *Background/Aim: Rapid glycolytic substrate-level phosphorylation (SLP) and accumulation of lactic acid are characteristics of diverse cancers. Recent advances in drug discovery have included the use of glycolytic inhibitors with mitochondrial targeting drugs to attempt to invoke an energy crisis in aggressive metabolically active chemo-resistant cancers. In this work, we examine the consequences of inhibiting mitochondrial oxidative phosphorylation (OXPHOS) with 1-methyl-4-phenylpyridinium (MPP+) in LS14T colon cancer cells containing a genetic double knock out (DKO) of lactic acid dehydrogenase (LDHA and LDHB). Materials and Methods: Several metabolic parameters were evaluated concomitant to whole transcriptomic (WT) mRNA, microRNA, and long intergenic non-coding RNAs using Affymetrix 2.1 human ST arrays. Results: MPP+ effectively blocked OXPHOS where a compensatory shift toward anaerobic SLP was only observed in the control vector (CV), and not observed in the LDH-A/B DKOs (lacking the ability to produce lactic acid). Despite this, there was an unexpected resilience to MPP+ in the latter in terms of energy, which displayed significantly higher resting baseline respiratory OXPHOS capacity relative to controls. At the transcriptome level, MPP+ invoked 1738 differential expressed genes (DEGs) out of 48,226; LDH-A/B DKO resulted in 855 DEGs while 349 DEGs were found to be overlapping in both groups versus respective controls, including loss of mitochondrial complex I (subunits 3 and 6), cell cycle transcripts and fluctuations in epigenetic chromatin remodeling systems. In terms of energy, the effects of MPP+ in the CV transcripts reflect the funneling of carbon intermediates toward glycolysis. The LDH-A/B DKO transcripts reflect a flow of carbons away from glycolysis toward the production of acetyl-CoA. Conclusion: The findings from this study suggest a metabolic resilience to MPP+ in cancer cells devoid of LDH-A/B, explainable in-part by higher baseline OXPHOS respiratory ATP production, necessitating more toxin to suppress the electron transport chain.*

The "Warburg effect" describes an abnormal metabolic phenotype of cancer cells relative to healthy adjacent tissue, evidenced by a high glycolytic rate, over-expression of glycolytic enzymes, a rise in lactic acid production, and a preference for fermentative aerobic glycolysis, with diminished oxygen use by the mitochondria (1). While the original understanding of the Warburg effects deduced a probable mitochondrial defect in cancer cells (2), the current understanding has evolved, particularly with the discovery that glycolytic inhibitors or lactic acid dehydrogenase (LDH) inhibitors such as NCI-066 merely shift metabolic reliance toward greater oxidative phosphorylation (OXPHOS)/ mitochondrial respiration and therefore more efficient production of ATP (3-5). In addition, high levels of oxygen and/or greater mitochondrial biogenesis drive tumorigenic processes (6-8) and appear to be prevalent in the stem cell metabolic phenotype (9, 10).

Interestingly, we have been studying the consequences of LDHA inhibitors for many years in diverse tumor cells and repeatedly failed to see any adverse effects on the production of lactic acid or tumor cell energy survival systems, with the only possible consequence being a reduction in cell proliferation (11-13). In collaboration with Dr. Jacques Pouyssegurs laboratory (Nice, France), our recent work further defined transcriptomic changes in colon cancer cells which were genetically engineered to knockout both LDHA/B genes (14), and in doing so, constructed a cell line

Correspondence to: Karam FA Soliman, Pharmaceutical Sciences Division, College of Pharmacy & Pharmaceutical Sciences, Institute of Public Health, Florida A&M University, Room G 134 H New Pharmacy Building, 1415 ML King Blvd, Tallahassee, FL 32307, U.S.A. Tel: +1 8505993306, e-mail: karam.soliman@famu.edu

Key Words: LDH, glycolysis, mitochondria, cancer cells.

lacking transcripts required to synthesize numerous LDH isoforms (15). That work was crucial in demonstrating the need to simultaneously down-regulate LDH-A and LDH-B genes in order to shut off the production of lactic acid in cancer cells. However, even with this, cancer cells remain immortal, experience slower doubling rates, and exhibit heightened mitochondrial OXPHOS capacity (15).

Findings such as these demonstrate a robust metabolic plasticity inherent to cancer cells that enable a continuous supply of energy produced by either or both glycolytic substrate-level phosphorylation (SLP) or mitochondrial oxidative phosphorylation (OXPHOS) to foster growth and metastasis under various micro-environments (16-18). Cancer cell metabolic rewiring is also a critical factor in driving chemo and radiation-resistant tumors (19, 20), where attempts have been made to combine chemotherapy drugs with metabolic inhibitors associated with anabolic fatty acid synthesis and catabolic oxidation [*e.g.*, stearoyl-CoA desaturase-1 (SCD1), ATP-citrate lyase (ACLY), acyl-coenzyme A synthetase short-chain family member 2 (ACSS2), acetyl CoA carboxylase (ACC), fatty acid synthase (FASN), and Carnitine palmitoyltransferase I (CPT1)](21-23). More recently, there has been a surge in experimentation involving the use of glycolytic or LDH inhibitors such as (IACS-010759) (4, 18) with mitochondrial based targets such as conjugated mitocan based triphenylphosphonium (TPP), BAY87-2243 with drugs such as the biguanide antidiabetics metformin or phenformin (3, 24, 25).

In this study we explore the metabolic consequences of using a well-known multi-complex mitochondrial complex I, IV inhibitor,1-methyl-4-phenylpyridinium (MPP+) in LDH-A/B DKO colon cancer cells which are devoid of the metabolic apparatus to carry out anaerobic glycolytic SLP (15).

Materials and Methods

Materials. Ninety-six well plates, Dulbecco's modified Eagle's medium (DMEM), fetal bovine serum (FBS), penicillin/streptomycin, general reagents, and supplies were all purchased from Sigma-Aldrich Co. (St. Louis, MO, USA) and VWR International (Radnor, PA, USA). All microarray equipment, reagents, and materials were purchased from Affymetrix/ Thermo Fisher (Waltham, MA, USA).

Cell culture. Dukes' type B, colorectal adenocarcinoma LS174T (ATCC® CL-188™) WT vector control (VC) *versus* LDHA/B double knock out (DKO) were established and kindly provided by Dr. Jacques Pouyssegur's facility at the University Cote d'Azur, Lacassagne, Nice, France (15). Cells were cultured in 75 cm^2 flasks with high glucose DMEM (4,500g/l) supplemented with 6% FBS and 100 U/ml penicillin G sodium and 100 μg/ml streptomycin sulfate. Cells were grown at 37˚C in 5% CO_2 and sub-cultured every three to five days. The CV had a rapid doubling time, produced high lactic acid levels, and grew in multi-cellular aggregates, which required trypsin detachment [Trypsin-EDTA (0.25%), phenol red] and pressurized distribution using a 5 ml serological pipette, and subsequent monolayer re-seeding. High glucose DMEM (4,500 mg/l) was used for all studies, except for monitoring studies to monitor glucose consumption. A switch to low glucose DMEM (1000 mg/l) was required to unmask rapid glucose utilization.

Cell viability. For basic experiments, cells were plated in 96 well plates at 0.5×10^6 cells/ml. Resazurin (Alamar Blue) indicator dye was used to measure cell viability/metabolic rate (26). Briefly, a working solution of resazurin (0.5 mg/ml) was prepared in sterile PBS, filtered through a 0.2-micron filter, added to the samples [15% (v/v) equivalent], and returned to the incubator for 2-6 hours. The data were quantified using a Synergy HTX multi-mode reader (Bio-Tek, Winooski, VT, USA) set on 530 nm (excitation) and 590 nm (emission) filters.

Lactic acid. Determination of cellular production of lactic acid produced was obtained using a colorimetric enzymatic assay with a lactate reagent according to the manufacturer (Trinity Biotech, Jamestown, NY, USA). The amount of lactic acid was measured in phenol red-free low serum media. The reagent was briefly added to the samples, incubated for 8 minutes, and quantified at 490 nm using a Synergy HTX multi-mode reader (Bio-Tek).

Glucose consumption. Briefly, cellular glucose consumption was quantified using an enzymatic assay comprised of glucose oxidase (20 U/ml) and a chromogenic solution and quantified at 490 nm on a Synergy/HTX multi-mode reader (Bio-Tek) as previously described (15). The data for glucose consumption was calculated as % of media blanks, housed in the first column of each 96 well.

Somatic cell ATP. Adenosine triphosphate (ATP) was assessed by using the adenosine 5'-triphosphate (ATP) bioluminescent somatic cell assay kit (Catalog Number FLASC) purchased from Sigma Aldrich (St. Louis, MO, USA) carried out according to the manufacturer's instructions. Briefly, the cells were lysed with ATP releasing reagent, transferred to a flat white bottom 96 well plate, and the data was quantified using the Synergy HTX multi-mode reader (Bio-Tek) set on luminescent measurement.

Oxygen consumption. A working solution of Janus Green (0.5 mg/ml) was prepared in sterile PBS and added to the samples [20% (v/v) equivalent]. Samples were then returned to the incubator to monitor differential profiles in the control group. Janus Green is a dye used to assess mitochondrial activity. As oxygen is consumed, the blue dye changes to a pink color and is quantified using a Synergy HTX multi-mode reader (Bio-Tek) with 530 nm (excitation)/590 nm (emission). Imaging was performed using an inverted fluorescent microscope under basic settings using the TRITC (red) filter cube.

NADH/NAD+. NADH/NAD+ cellular concentrations were determined according to the manufacturer's protocol (Sigma #MAK037 NADH/NAD determination kit), and data were quantified using the optical density on a Biotek Synergy Multi-Mode Reader. NADH concentrations were subtracted from the total NAD+ and NADH values to obtain NAD+, and data were calculated as a total ratio.

Lipids. According to the manufacturer's guidelines, lipid isolation was carried out using several methods, including a slight modification of the Folch's extraction procedure consisting of a biphasic solvent system of chloroform/methanol/water in a volumetric ratio of 8:4:3 (v/v/v). All lipid studies were carried out under ahigh–fed state with ample glucose supply.

Cholesterol esters. Briefly, the cells were scraped, washed 3x with cold PBS, and pelleted into micro-centrifuge tubes. 440 µl of isopropanol, 280 µl of chloroform, and 40 µl of NP-40 solution were added to each pellet and samples were homogenized for 30 seconds, spun at 15,000 × *g* for 10 minutes at 4˚C and the organic phase transferred to a new tube, then dried at 50˚C. The determination of cholesterol/ cholesteryl esters was carried out using Abcam product #ab102515 (Cambridge, MA, USA) according to the manufacturer's guidelines and quantified using a Synergy HTX multi-mode reader (Bio-Tek) with 530 nm (excitation)/590 nm (emission).

Triglycerides. Briefly, the cells were scraped, washed 3× with PBS, and pelleted into microcentrifuge tubes. According to the manufacturer guidelines, triglycerides were determined using Abcam product #ab65336. After adding NP-40 solution and subjecting the samples to a series of heat cycles at 100˚C, the upper layer was combined with assay buffer and lipase, placed on a rocker shaker for 20 minutes, followed by addition of a detection reagent, incubation for 1 hour and quantification using a Synergy HTX multi-mode reader (Bio-Tek) with the following settings: 530 nm (excitation)/590 nm (emission).

Neutral lipids. Briefly, the cells were scraped, washed 3× with PBS, and pelleted into microcentrifuge tubes. According to the manufacturer guidelines, neutral lipids were determined using Abcam #ab242307. After pelleting, 200 µl methanol and 400 µl, chloroform was added before homogenization. 150 µls of pure water was added to the samples, followed by vortexing and centrifuging at 1000 × *g* for 5 min. Approximately 150 µl of the lower layer was isolated into a glass vial and left to evaporate (55˚C), then reconstituted to 150 µl with isopropanol. Subsequently, 40 µls of that sample was collected, and neutral lipids were determined using Abcam #ab242307 carried out according to the manufacturer guidelines. Neutral lipids were quantified using a Synergy HTX multi-mode reader (Bio-Tek) with the following settings: 480 nm (excitation)/580 nm (emission).

Microarray WT 2.1 human datasets. After the experimental treatment, the cells were scraped, washed three times in ice-cold HBSS, spun down, the supernatant removed, and the remaining pellet was rapidly frozen and stored at –80˚C. Total RNA was isolated and purified using the Trizol/chloroform method. The RNA quality was assessed, and concentrations were equalized to 82 ng/µl in nuclease-free water. According to the GeneChipTM WT PLUS Reagent Manual for Whole Transcript (WT) expression arrays, whole transcriptome analysis was conducted. Briefly, RNA was reverse transcribed to first strand /second strand cDNA followed by cRNA amplification and purification. After 2nd cycle ss-cDNA Synthesis and hydrolysis of RNA, ss-cDNA was assessed for yield, fragmented, labeled, and hybridized onto the arrays before being subjected to fluidics and imaging using the Gene Atlas (Affymetrix, ThermoFisher Scientific). The array data quality control and initial processing from CEL to CHP files were conducted using an expression console before data evaluation, using the Affymetrix transcriptome analysis console, String Database (String Consortium 2020), and DAVID functional annotation microarray tools (27-29). The dataset has been deposited to NIH Gene Expression Omnibus located at https://www.ncbi.nlm.nih.gov/geo/query/acc.cgi?acc=GSE149289.

Data analysis. Statistical analysis was performed for basic studies using GraphPad Prism (version 3.0; Graph Pad Software Inc., San Diego, CA, USA). Significant differences between the groups were assessed using either the student's *t*-test or one-way ANOVA, followed by Tukey's *post hoc* analysis.

Results

The effects of MPP+ (0.014-7.4 mM) on basic metabolic parameters in both control vectors (CV) (Figure 1A) and LDH-A/B DKO cells (Figure 1B) were determined, including viability/metabolic rate, ATP, cell respiration, glucose use, and lactic acid production. The study's high glucose requirement (4,500 mg/l) in Figure 1 becomes a critical control issue because a high plating cell density in a micro-titer plate containing finite glucose, when employing a mitochondrial toxin, will trigger rapid glycolysis/ exhaustion of glucose supplies and therefore indirect cell death. The effects of MPP+ observed in the CV are well within the bounds of what we have observed in diverse cancer cells over the years (Figure 1A) (30). This includes a compensatory reliance on SLP in glycolysis to sustain ATP levels coinciding with the rise in lactic acid and a gradual accelerated decline in glucose concentration. We anticipated that treating the LDH-A/B DKO cells with MPP+ would be catastrophic, simply because blocking both OXPHOS and SLP should evoke an energy crisis. However, on the contrary, the death curve in the LDH-A/B was relatively mild, with very little difference from the CV, as shown in Figure 1A. After repeating this work several times, we ultimately figured that the baseline differential between the CV of Figure 1 is inherently different from the LDH-A/B DKO in terms of OXPHOS resting capacity, shown as % control. In Figure 2A, we show the resting differential in OXPHOS between the CV and the LDH-A/B DKO by relative fluorescence and corresponding images evaluated with Janus Green: B (1) CV and B (4) LDHAB-DKO, where it becomes evident that the cellular respiration rate of the LDA-A/B DKO cell lines is amplified at baseline. Here we show that the CV group mitochondria are very close to being completely shut down by 116 µM of MPP+ [Figure 2B (2)] and fully suppressed at 463 µM [Figure 2B (3)].In contrast, in the LDH-A/B DKO, even at 1.8 mM MPP+, the cells are still respiring, which coincides with the data obtained in Figure 1.

Further studies were conducted to determine the inherent metabolic differences between the CV and the LDH-A/B DKO in resting untreated cells (Figure 3). The data show that the CV uses glucose rapidly and produces abundant lactic acid (Figure

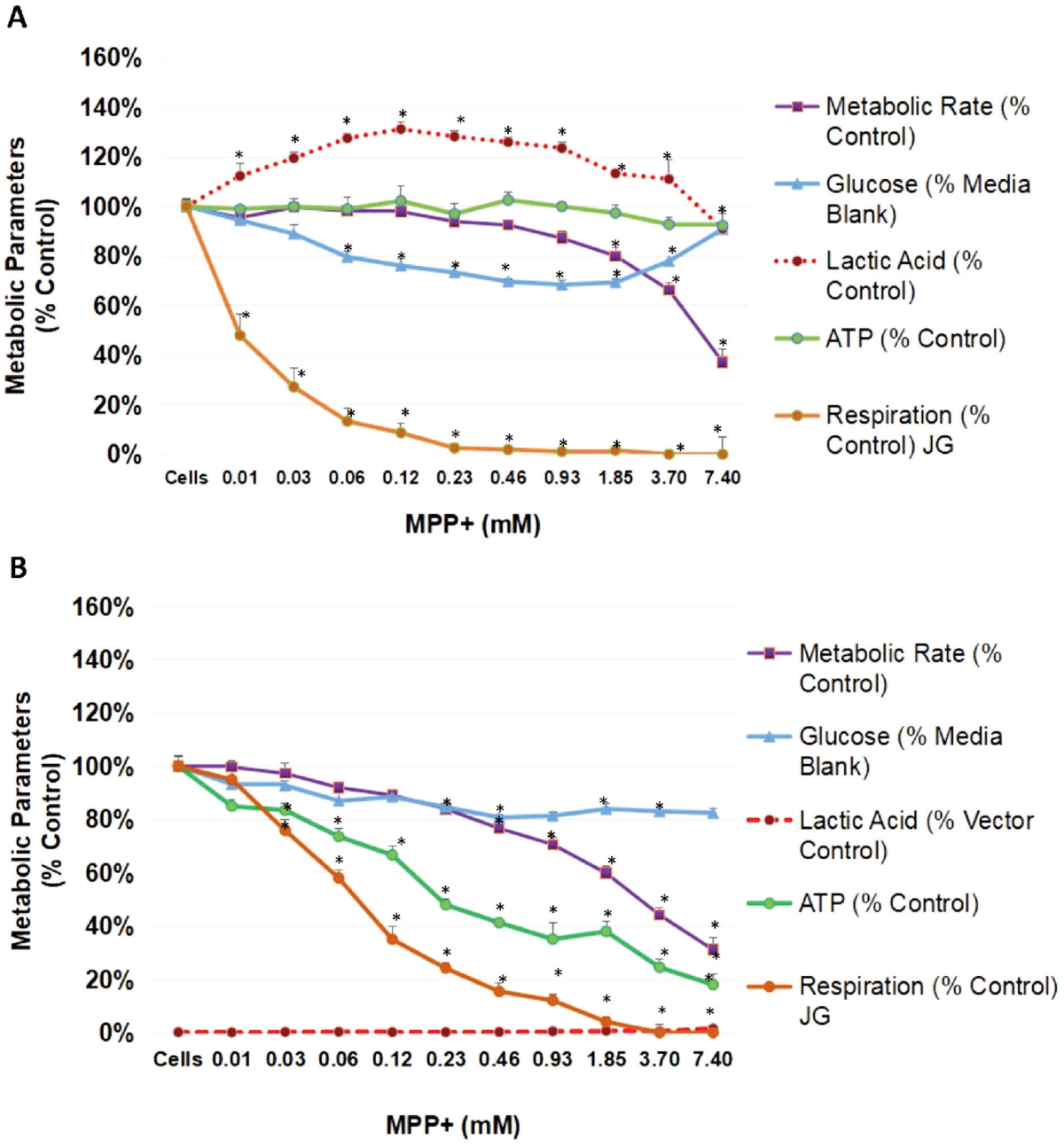

Figure 1. *Metabolic profile of response to MPP+ (0.014-7.4mM) in the control vector (CV) (1A) vs. LDHA/B-DKO LS174T cells cultured in high glucose media (1B). The data represents the mean ± SEM, n=4 for metabolic rate (viability) as % control, glucose utilization as % of glucose concentrations in a media blank, lactic acid production as % of lactic acid in the CV cell line, cell respiration as % of control and ATP produced as % of control. Significant differences between the control and MPP+ treatment was determined by a one-way ANOVA, followed by a Tukey post hoc test, *p<0.05.*

3A), which is opposite to the LDH-A/B DKOS, which show little to no glucose use, and a complete absence of lactic acid. Even though there was a dramatic metabolic divergence between how the CVs and LDH-A/B DKOs produce energy, the NADH to NAD+ ratio appears to follow a steady-state equilibrium (Figure 3B). The basic lipid profiles between the two cell lines do not vary significantly under a high glucose fed state for either neutral lipids or cholesterol esters (Figure 4B, C) with a slight increase in intracellular triglycerides (Figure 4A). As to the direct involvement of metabolic rewiring

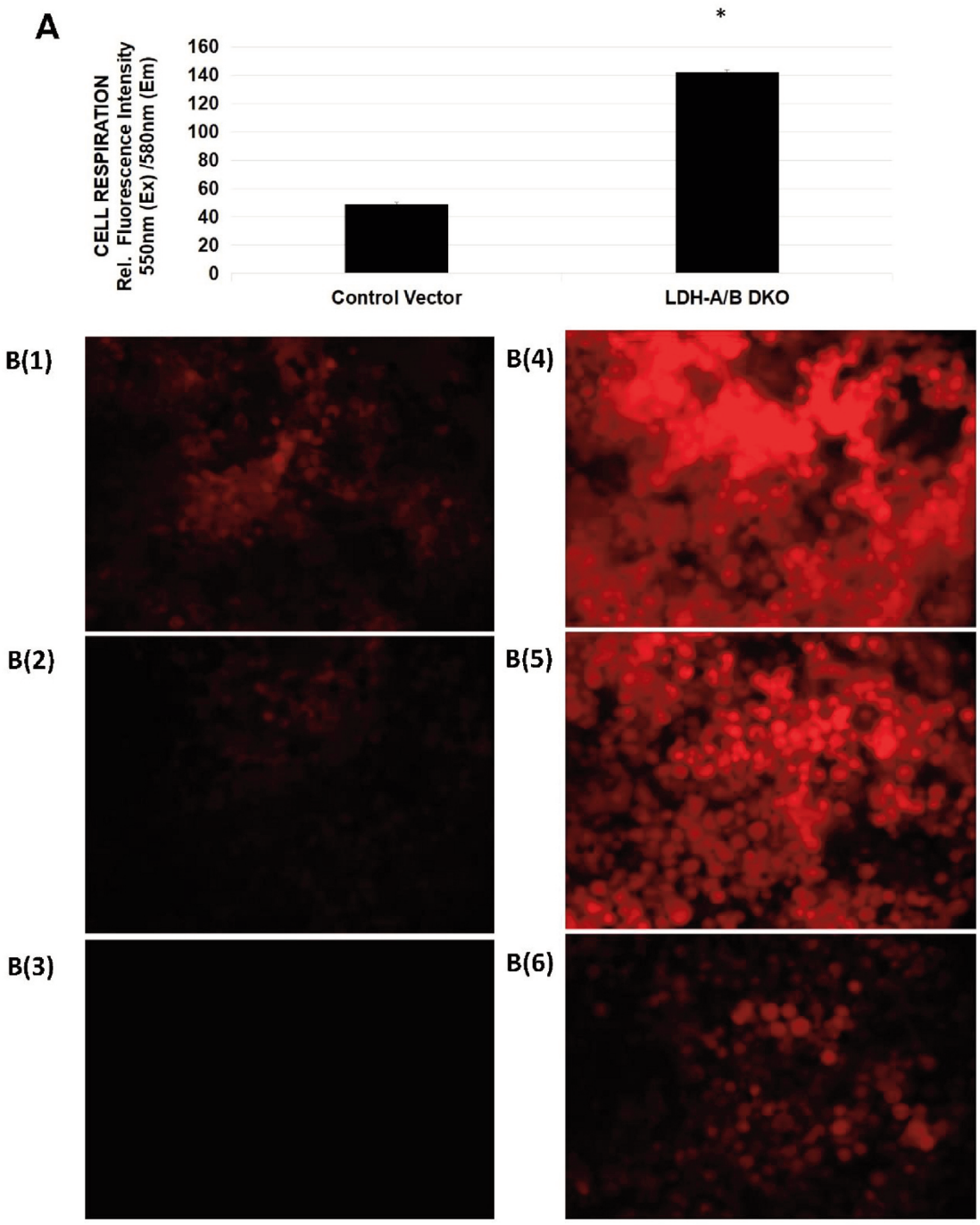

Figure 2. *Differential cellular respiratory profile in the CV vs. LDH-A/B DKO LS174T cells cultured in high glucose media. The data are expressed as mean±SEM, n=4, for cell respiration with significant differences between the CV and the LDH-A/B DKO determined by student's t-test, *p<0.05, n=4. (A) Fluorescent images represent higher intensity (cellular respiration). (B), where the data represent B (1): (CV), B (2): CV with 116 μM MPP+, B (3): CV with 463 μM MPP+, B (4): LDH-AB/DKO controls, B (5): LDHA/B DKO with 463μM MPP+ and B (6): LDHAB DKO with 1.8 mM MPP+.*

in the LDH-A/B DKO resting *vs*. CV to use fats for energy, further studies will be required to understand this aspect fully.

Next, optimal concentrations of MPP+ were established to conduct comparative microarray transcriptomic analysis, which we set at 231 μM MPP+, n=3 (Figure 5). An overall summary of differentially expressed genes (DEGs) evoked by MPP+ in CV or LDH-A/B DKOs was conducted. Out of 48,226 gene transcripts tested, there were 1738 DEGs by

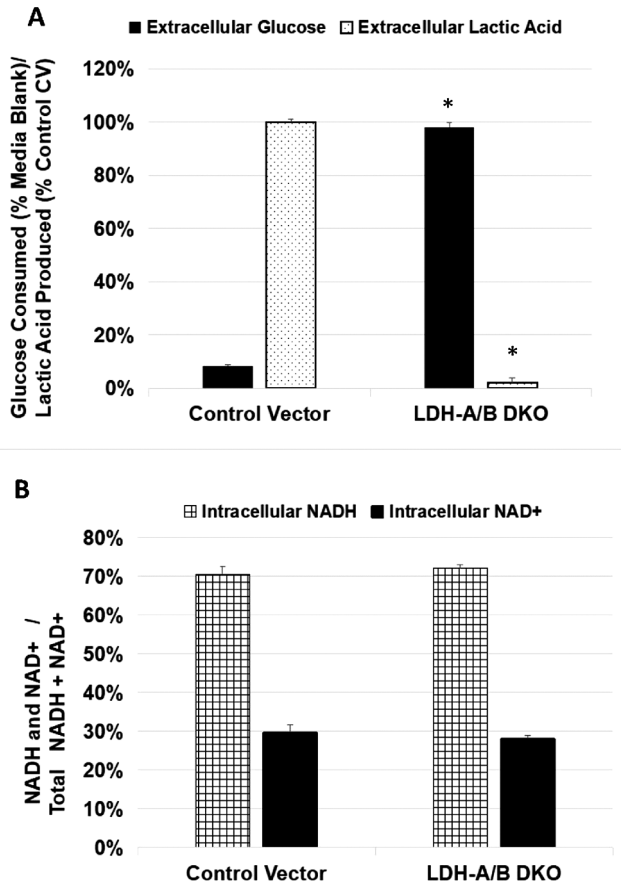

Figure 3. *Differential glycolytic profile in the CV vs. LDH-A/B DKO LS174T when cultured in low glucose media. (A) The data are expressed as mean±SEM, n=4 for glucose consumed relative to media blank (% media blank control) and lactate produced relative to % lactate released in the control vector. Significant differences between the vector control and LDH-A/B DKO were determined by a student's t-test, *p<0.05. Differential redox in CV vs. LDH-A/B DKO LS174T cells cultured in high glucose media. (B) The data are expressed as mean±SEM, n=4 for NADH and NAD+ as relative % of the total combined NADH+NAD+ concentrations. Significant differences between the vector control and LDH-A/B DKO were determined by student's t-test, p<0.05, NS.*

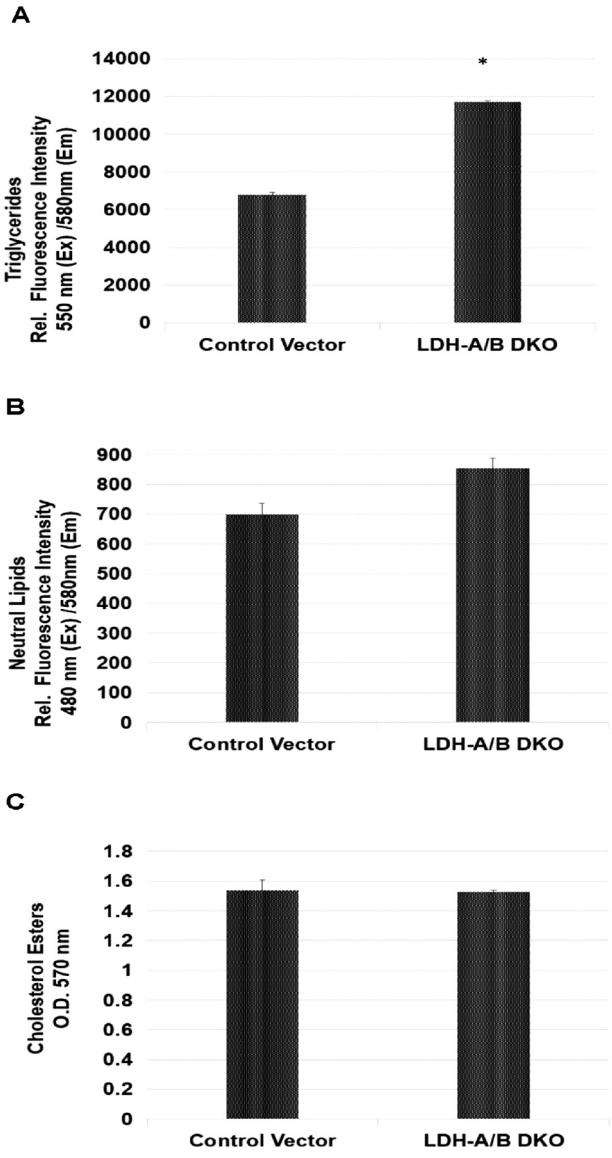

Figure 4. *Differential lipid profiles for the CV vs. LDH-A/B DKO LS174T cells cultured in high glucose media. The data are expressed as mean±SEM, n=4 as relative fluorescence for (A) Neutral Lipids and (B) Triglycerides and optical density for (C) cholesterol esters. Significant differences between the vector control and LDH-A/B DKO were determined by student's t-test, *p<0.05.*

MPP+ in the CV group and 855 DEGs by MPP+ in the LDHA/B - DKO group. Of these changes, MPP+ caused very similar changes in both groups for 79-up-regulated genes and 270 down-regulated ones. The largest DEG reduction for MPP+ in both groups was HIST1H2BM (-9.16 FC, FDR- p=0.0000621, Control Vector) and (-136.76 FC, FDR - p=0.0000011, LDH-A/B DKO).

Using the String interactive database, we looked at overlapping DEGs in the CV and the LDH-A/B DKO group evoked by MPP+ on OXPHOS related processes. MPP+ down-regulated several mitochondrial-related genes, including transcripts coding sub-units of NADH dehydrogenase (Complex 1), mitochondrial outer compartment and fatty acid metabolism genes (Figure 6). More specifically, in both groups MPP+ reduced cytochrome b (CTYB), ATPase, class V, type 10A (ATP10A), NADH dehydrogenase, subunit 3 (complex I) (ND3) and NADH dehydrogenase, subunit 6 (complex I) (ND6) (Refer to NIH Gene Expression Omnibus located at: https://www.ncbi.nlm.nih.gov/geo/query/acc.cgi?acc=GSE149289).

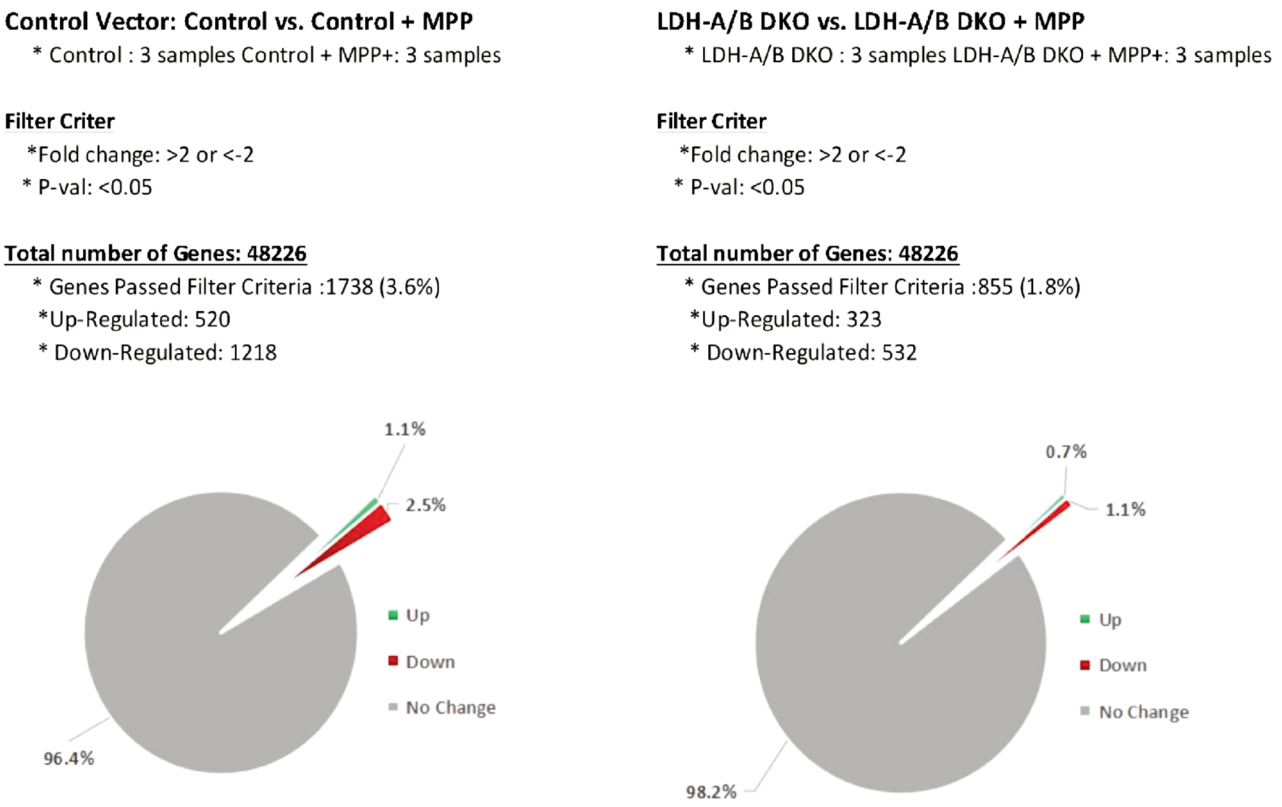

Figure 5. *Human transcriptome summary report for CV vs. CV+ MPP+ and LDH-A/B DKO vs. LDH-A/B DKO + MPP+. The summary of differentially expressed genes (DEGs) from the total number of genes evaluated; 48,226 using Affymetrix 2.1 ST Human Arrays. There were 416 overlapping DEGs of the same gene when treated by MPP+ in control vs. LDH-A/B DKOs.*

In response to MPP+, the global transcriptome differential expression for both groups ± MPP+ are shown by the volcano plot summary in Figure 7 (CV) and Figure 8 (LDH-A/B DKO). Using the DAVID comprehensive functional annotation bioinformatics array analysis tools, we provide the most significantly impacted biological systems by MPP+ in both groups (CV and LDH-A/B DKO) (Table I). It is evident that in both groups, MPP+ caused a down-regulation of transcripts which are essential for cell division, progression through the cell cycle, DNA replication, DNA strand elongation and excision repair, underscored by large changes in the epigenetic activity (Table I, Annotation cluster 8 and 14).

These changes were also observed using the Affymetrix transcriptome analysis (TAC) Wiki pathway analysis tool describing the effects of MPP+ on the CV (Figure 9) and the LDH-A/B DKO cell line (Figure 10). MPP+ caused significant changes to everything from the origin recognition complexes, minichromosomal maintenance complexes, and genes involved with each of the four phases of the cell cycle (G1, S, G2, and M). With very few up-regulatory DEGS in both groups by MPP+, DAVID analysis tools fall short of providing solid enrichment scores but rather indicate a probability of stress-related genes (Table II). Refer to the data located in NIH Gene Expression Omnibus at https://www.ncbi.nlm.nih.gov/geo/query/acc.cgi?acc=GSE149289.

Next, we provide the unique DEG profiles elicited by MPP+ being specific to only the LDH-A/B DKO cell lines in Table III with ** denoting elements incorporated into the discussion regarding the differential transcriptomes related to glycolysis, the TCA cycle and reducing equivalents shuttled to the mitochondria. A general schematic is presented in Figure 11. These findings provide a basic platform for future analysis into understanding how cancer cells might overcome such dramatic simultaneous insult to both OXPHOS and SLP.

Discussion

Biological response to hypoxia, anoxia, or mitochondrial impairment in eukaryotes involves a compensatory shift toward anaerobic glycolysis, which sustain ATP through substrate level phosphorylation (SLP), resulting in accumulation of lactic acid. SLP is strictly dependent upon the function of lactic acid

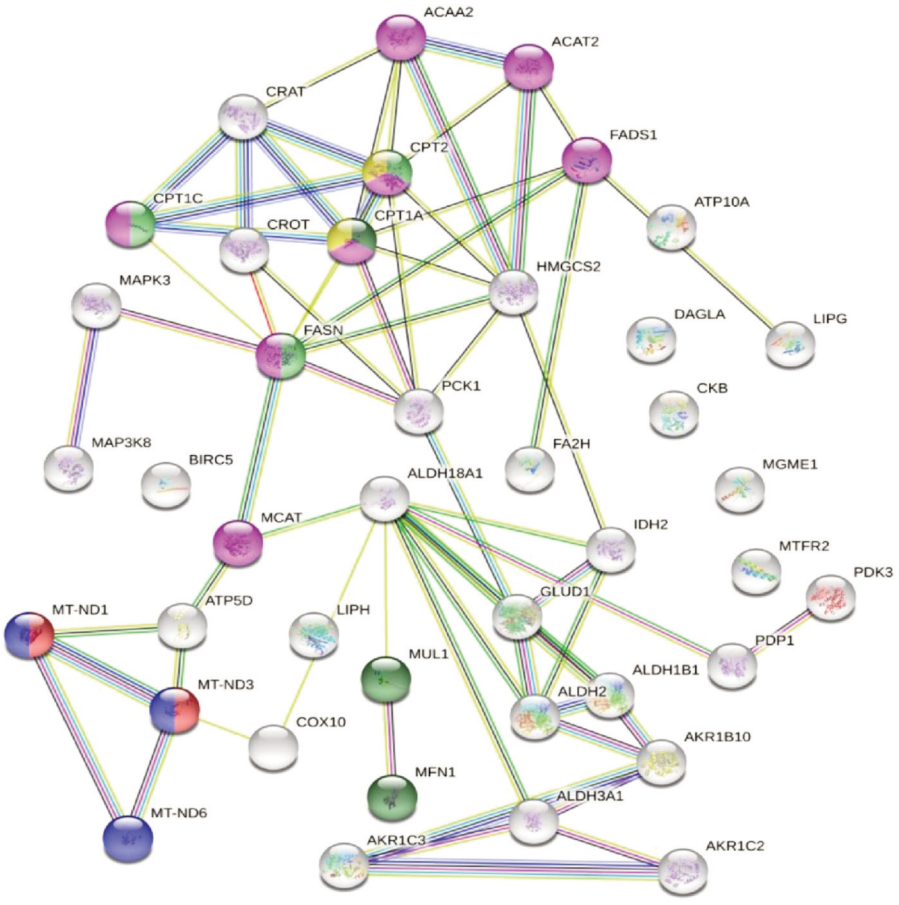

ID	Go-Term	Description	Count in Network	Strength	FDR	Color Code
	Cellular Component (Gene Ontology)					
GO-Term	GO:0031307	Mitochondrial Member (Outer Component)	3 of 23	1.79	0.0003	
GO-Term	GO:0005747	Mitochondrial Complex I (NADH Dehydrogenase)	2 of 46	1.32	0.024	
GO-Term	GO:0070469	Respiration	3 of 93	1.19	0.0065	
	Local network cluster (STRING)					
Cluster	CL: 21473	Mitochondrial Member (Outer Component)	3 of 23	1.79	0.0005	
	KEGG Pathways					
Pathway	hsa01212	Fatty Acid Metabolism	8 of 48	1.9	1.86E-11	
	Reactome Pathways					
Pathway	HSA:200425	Import of Palmitoyl-CoA into the mitochondrial	2 of 14	1.83	0.007	

FDR = False Discovery Rate, **Color Code** = String Mode Ball Gene Symbol Match

Figure 6. *Mitochondrial, energy-related genes altered by MPP+ in both the CV and LDH-A/B DKO sets as determined by the Protein-Protein Interactive String Database Analysis. The data are presented as gene symbol (circular) and color-coded (circular), specifically for mitochondrial related and energy processes listed in the results. White-colored nodes are presented for REDOX and apoptotic related genes.*

dehydrogenase (LDH) in order to convert pyruvate to lactic acid to generate oxidized NAD+ to drive ATP production through phosphoglycerate kinase and pyruvate kinase. However, in cancer cells, even in the presence of normoxia or hyperoxia, there is predominant glycolytic activity and lactic acid accumulation, originally believed to involve a defect in mitochondria and referred to as the Warburg effect (31, 32). Recently, there has been a paradigm shift due to advances in

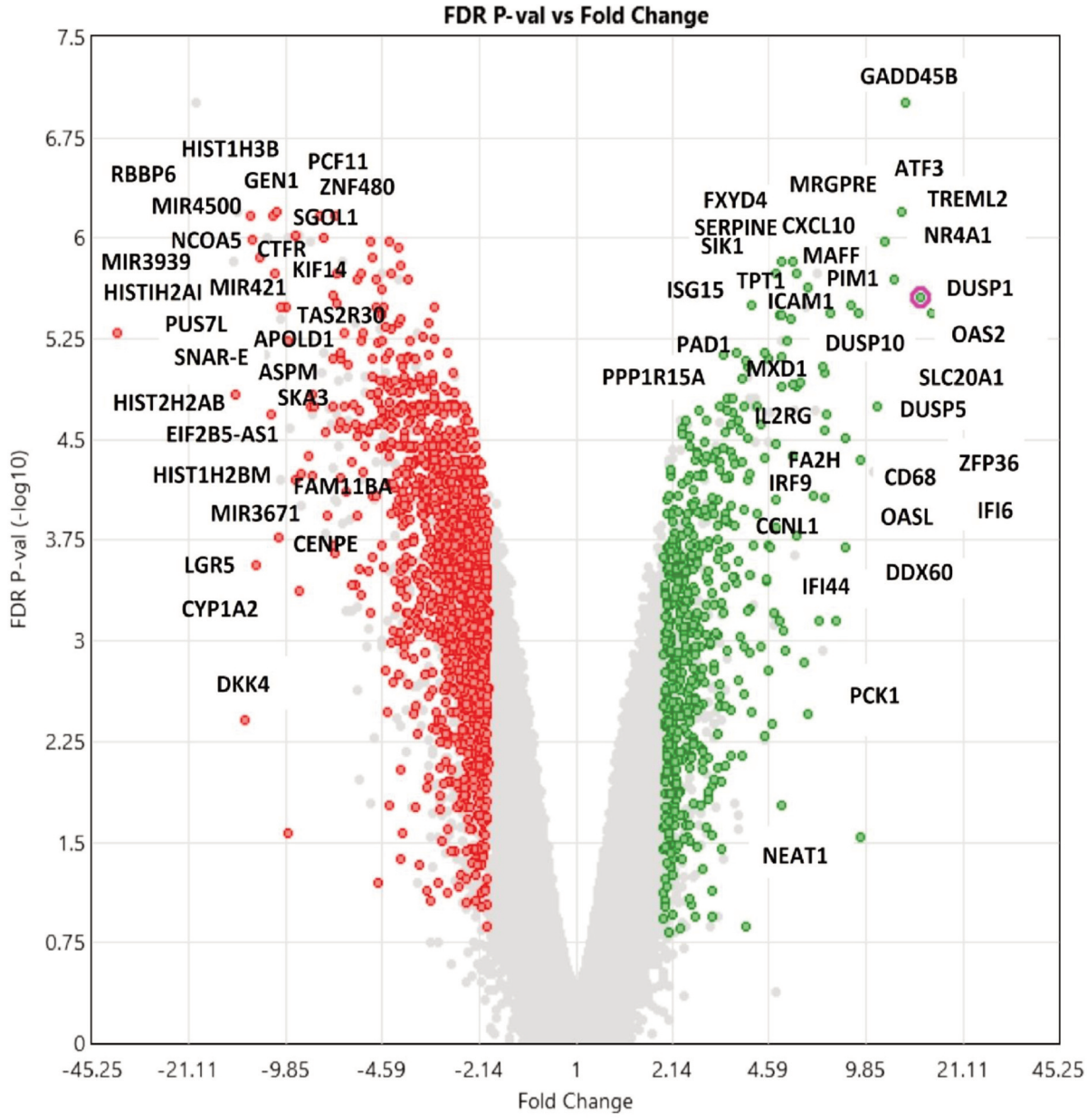

Figure 7. *Whole transcriptomic DEG profile of the Control vector LS174T cells ± MPP+. The data is expressed in a volcano plot providing information on fold change (X-axis) and FDR p-Value (Y-axis). The graph contains select gene symbols for the most highly affected genes.*

cancer research. First, the Warburg effect is not necessarily a function of faulty mitochondria, but one of its main purposes is to sustain tumor microenvironment acidity (33), which is paramount to invasive metastasis, chemo resistance and immune escape (34, 35). Secondly, while the mitochondrial electron transport chain (ETC) and OXPHOS is required to sustain tumor growth and ATP production when needed (33, 36, 37), high levels of either oxygen and/or greater mitochondrial biogenesis will drive tumorigenic processes as evidenced by perioperative surgical, experimental models (6-8) and investigation of stem cell metabolism (9, 10). While previous therapeutic attempts have involved experimenting with glycolytic inhibitors (38), a fairly new area of anti-cancer therapy now includes deployment of mitochondria-targeted therapeutics, however challenges in using classical inhibitors of OXPHOS are not without counter-indication, as mitochondrial inhibitors have a long history of contributing to degenerative diseases such as Parkinson's or Alzheimer's disease (39, 40).

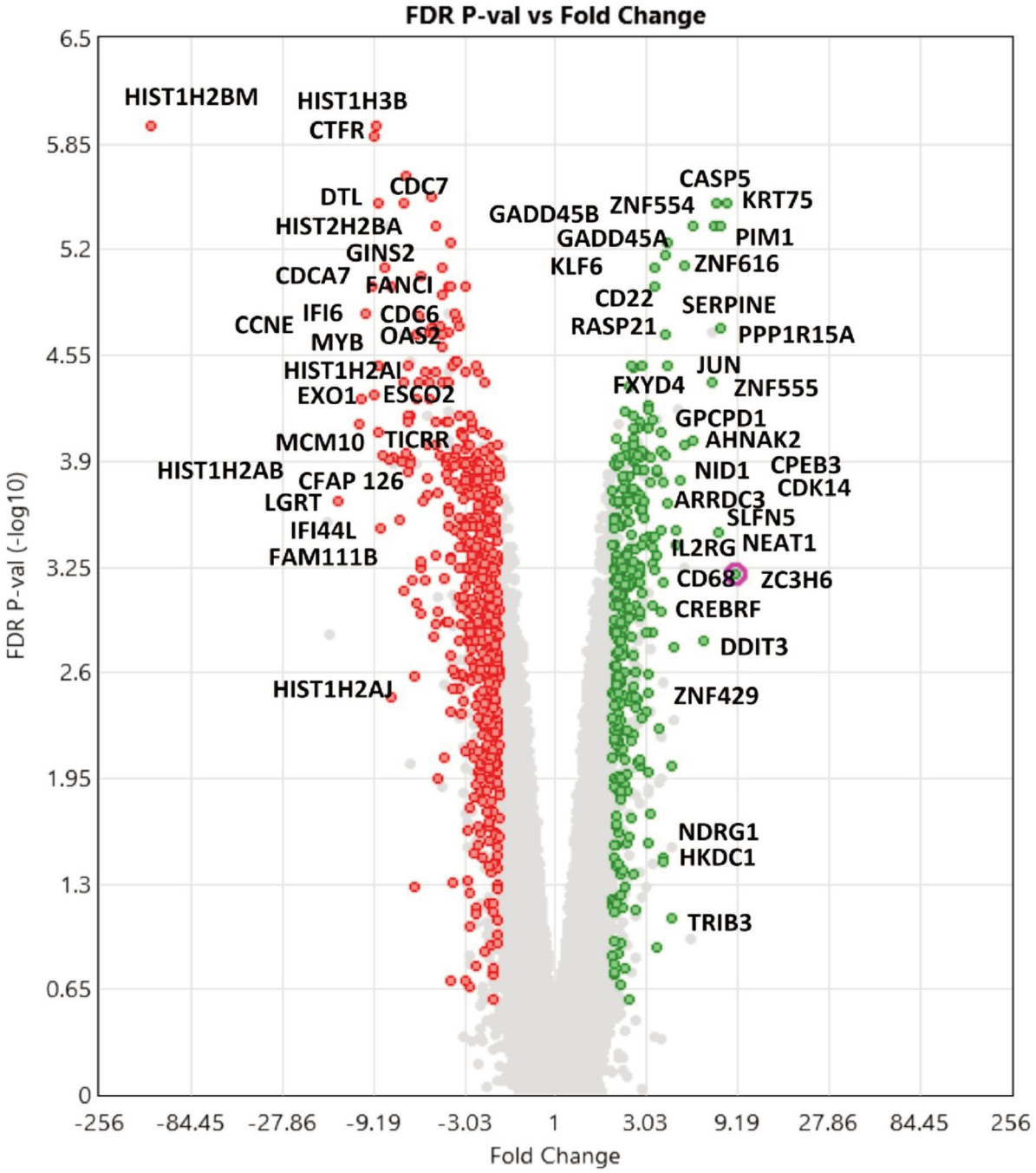

Figure 8. *Whole transcriptomic DEG profile of the LDH-A/B DKO LS174T cells ± MPP+. The data is expressed in a volcano plot providing information on fold change (X-axis) and FDR p-Value (Y-axis). The graph contains select gene symbols for the most highly affected genes.*

A rationale for the use of mitochondrial inhibitors to treat cancer was instituted by cause-effect linked observation where reduced tumor growth occurred in individuals using various drugs with mitochondrial inhibiting properties such as anesthetics. Several types of anesthetics (complex I,II,III and IV inhibitors), such as propofol, ropivacaine and bupivacaine reduce mitochondrial biogenesis, PGC-1alpha (41-43) and accelerate glycolysis exerting reduced tumor growth and augmented chemotherapeutic efficacy (44-47) similarly, silencing critical OXPHOS related genes such as

Table I. *DAVID functional annotation pathway analysis of down-regulated- DEGs caused by MPP+ when comparing Controls vs. Controls + MPP+ and LDH-A/B DKO vs. LDH-A/B DKO + MPP+. The data represents enrichment score, biological classifications, DEG count, p-Value, and Benjamin False Discovery p-Value.*

Cluster	Enrichment score	#Genes	Significance	
Annotation Cluster 1	Enrichment Score: 38.7	Count	*p*-Value	Benjamini
	Cell cycle & Mitosis	78	4.10E-56	9.30E-54
Annotation Cluster 2	Enrichment Score: 22.82	Count	*p*-Value	Benjamini
	Chromosome, Chromatid, Centromeres, Kinetochores	55	9.30E-42	1.10E-39
Annotation Cluster 3	Enrichment Score: 22.77	Count	*p*-Value	Benjamini
	DNA Replication, G1/S Transition Mitosis	29	4.80E-32	1.80E-30
Annotation Cluster 4	Enrichment Score: 18.97	Count	*p*-Value	Benjamini
	DNA Damage	36	1.50E-22	3.80E-21
Annotation Cluster 5	Enrichment Score: 6.97	Count	*p*-Value	Benjamini
	ATP Binding	42	3.50E-08	3.80E-07
Annotation Cluster 6	Enrichment Score: 6.69	Count	*p*-Value	Benjamini
	ATPase Domain Binding	13	8.00E-08	9.00E-06
Annotation Cluster 7	Enrichment Score: 6.34	Count	*p*-Value	Benjamini
	Fanconi anemia pathway (DNA repair)	10	3.30E-08	7.50E-07
Annotation Cluster 8	Enrichment Score: 5.46	Count	*p*-Value	Benjamini
	Epigenetics: Chromatin, Methylation, Nucleosome Remodeling, Histone Core & folds, citrullination, H2A, H3.1, H3.2, H3,	18	3.10E-15	1.90E-13
Annotation Cluster 9	Enrichment Score: 5.23	Count	*p*-Value	Benjamini
	DNA Replication/MCM Helicase, MCM Complex	8	2.50E-08	8.70E-07
Annotation Cluster 10	Enrichment Score: 5.13	Count	*p*-Value	Benjamini
	DNA strand elongation, replication, damage repair, translation, DNA Polymerase, nucleotide excision repair	14	5.00E-16	2.20E-14
Annotation Cluster 11	Enrichment Score: 4.62	Count	*p*-Value	Benjamini
	DNA strand replacement, recombination, reciprocal meiotic recombination, lateral element, recombinase, double-strand break reprocessing	13	1.80E-14	1.60E-12
Annotation Cluster 12	Enrichment Score: 4.26	Count	*p*-Value	Benjamini
	Cyclins, P53 Signaling Pathway	6	1.50E-06	5.30E-05
Annotation Cluster 13	Enrichment Score: 3.67	Count	*p*-Value	Benjamini
	Microtubule movement, Kinesins-motor regions, retrograde Golgi to ER	19	5.60E-09	6.70E-08
Annotation Cluster 14	Enrichment Score: 2.83	Count	*p*-Value	Benjamini
	Epigenetics: H4, histone Binding, silencing at rDNA, TAF, beta catenin-TCF complex assembly	10	2.10E-08	5.00E-07
Annotation Cluster 15	Enrichment Score: 2.25	Count	*p*-Value	Benjamini
	HHH2, Helix-hairpin-helix motif, class 2, XPGN	3	8.40E-04	4.10E-02
Annotation Cluster 16	Enrichment Score: 2.09	Count	*p*-Value	Benjamini
	Purine, Pyrimidine, DNA Polymerases	4	4.00E-05	3.50E-04
Annotation Cluster 17	Enrichment Score: 2.08	Count	*p*-Value	Benjamini
	Protein Phosphatase (tyrosine)	7	1.30E-05	4.20E-04

S100 calcium-binding protein A4 (S100A4) will reduce OXPHOS, complex I and ATP, accelerate glycolysis and attenuate invasive metastatic tumorigenesis in a three-dimensional growth models or *in vivo* (48). This pattern also extends to cardiac drugs (*e.g.* atovaquone; complex III inhibitor) (2) and anti-diabetic drugs such as the biguanide metformin or phenformin (complex I inhibitor), which attenuates mitochondrial respiration, amplifies glycolysis and results in reduced tumor growth in diverse models such as lymphoma (49-51). Phenformin has a history of causing lactic acidosis, which was in some cases fatal, justifying removal from the US drug market (52, 53). In the case of metformin, lactic acidosis is not as severe and is considered fairly safe (54) with potential drug repurposing application to treat diverse human cancers (55, 56). Oddly, in vitro experimental models using cancer cells to investigate the efficacy of metformin + glycolytic inhibitors such as 2-DG, require relatively high concentrations to confer symbiotic effects

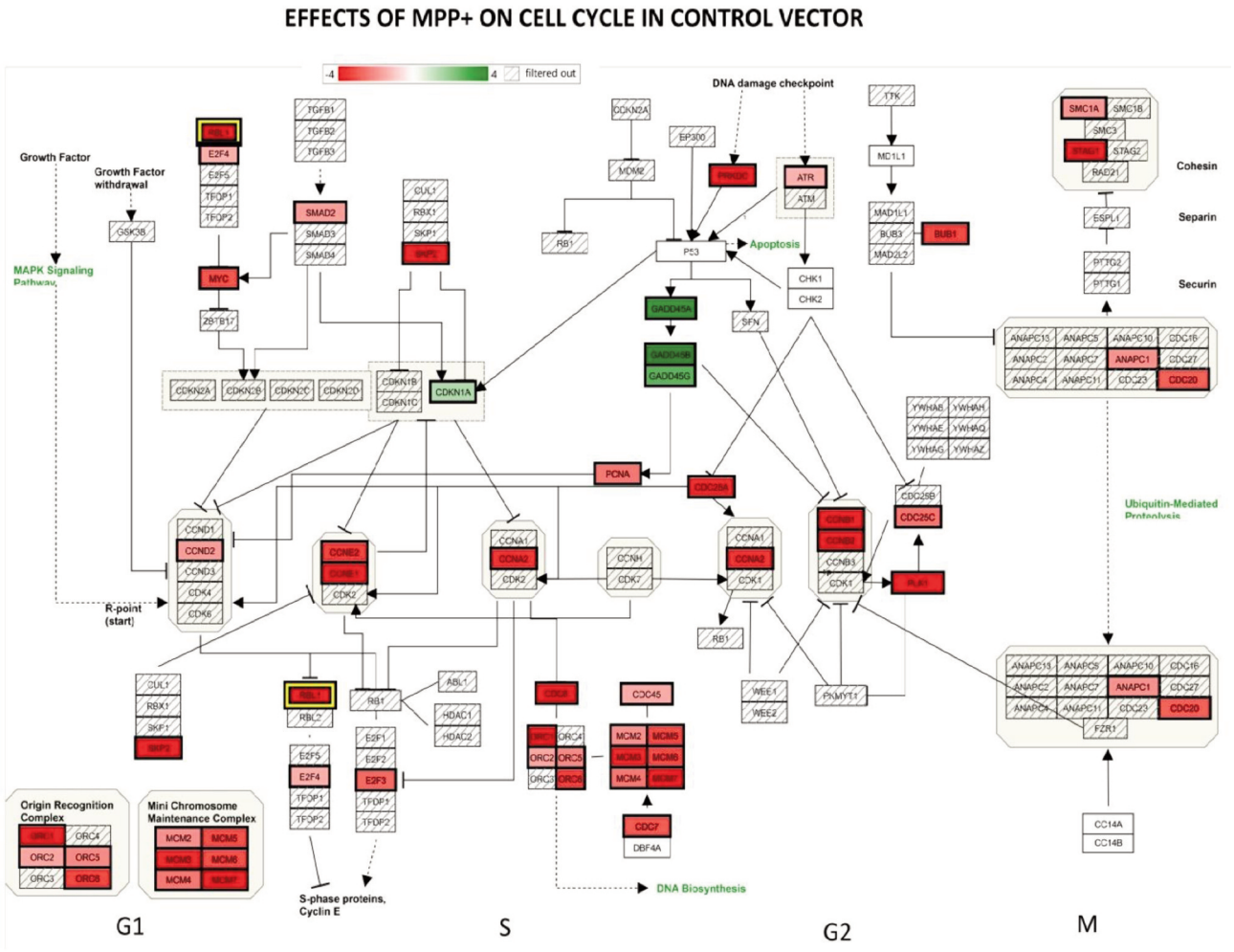

Figure 9. *Affymetrix transcriptomic analysis of down-regulated- DEGs caused by MPP+ in Control Vector (Figure 8A) and LDHA/B-DKO (Figure 8B) collectively involved with cell cycle arrest. Green, up-regulated DEG; red, down-regulated genes.*

(high uM –low mM) (49, 57, 58). For this reason, there has been a recent surge in rationale and design of sophisticated conjugated cationic lipophilic mitochondrial carries that carry drugs such as metformin directly to the mitochondria in tumor cells (*e.g.* Mito-Met10), which can drastically alter the efficacy of a drug such as metformin by approximately 400 fold (59). The use of mitochondrial cationic lipophilic carriers, are central to today's mitochondrial targeting therapies which work by taking advantage of tumor specific depolarized plasma membrane potentials/ acidic pH+ coupled to mitochondria negatively charged or hydrophilic polymer-stabilized nano-carries to access the mitochondria. These carrier backed systems include attaching diverse drugs to a cationic lipophilic carrier such as triphenylphosphonium (TPP+) or mitoquinone (Mito-Q) coenzyme Q + TPP+, housing conjugated mitochondrial inhibitors (Complex I-III inhibitors, ATP synthase inhibitors, or uncoupling agents), chemotherapy drugs, antioxidants, some of these have been combined with glycolytic inhibitors such as 2-deoxyglucose (2-DG) (60, 61)(62-64) . Other cations that can be used as cancer specific theranostic imaging or conjugated to a variety of other moieties including dequalinium (DQA), guanidine, Mito-carboxy proxyl (Mito-CP), pyridinium, 3-phenylsulfonylfuroxan, or (E)-4-(1H-indol-3-ylvinyl)-N-methylpyridinium iodide (F16) which can carry with them a variety of drugs (*e.g.* chlorambucil, vitamin derivatives, or metformin) (62, 65-68) to inhibit tumor growth (62, 69).

In the current study, we directly employ the use of MPP+ to inhibit the mitochondria because it a well-known complex I and IV inhibitor, with the capacity to both reduce transcripts that encode mitochondrial enzymes as well as being eliciting kinetic inhibition of cytochrome oxidase (70-73). Here we treat colon cancer cells with MPP+ either without the LDH-A/B gene or a control set, the former

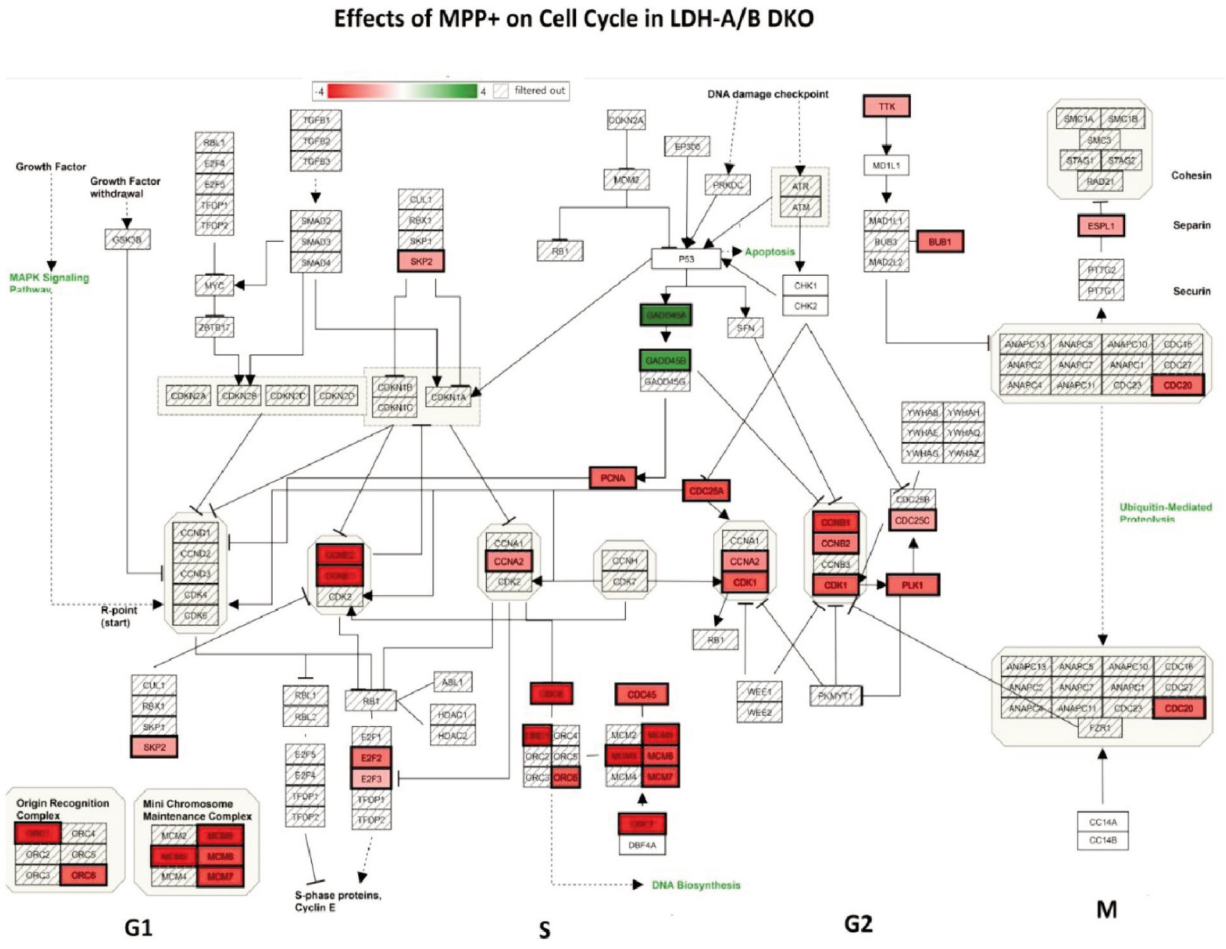

Figure 10. *Affymetrix transcriptomic analysis of upregulated DEGs caused by MPP+ when comparing Controls vs. Controls + MPP+ and LDH-A/B DKO vs. LDH-A/B DKO + MPP+. The data represents FC (p<0.05), where DEGs were far greater in controls than LDH-A/B DKO (black - right) and greater in LDH-A/B DKO than controls on the left (Red).*

Table II. *DAVID functional annotation pathway analysis of up-regulated DEGs caused by MPP+ when comparing Controls vs. Controls + MPP+ and LDH-A/B DKO vs. LDH-A/B DKO + MPP+. The data represents enrichment score, biological classifications, DEG count, p-Value, and Benjamin False Discovery p-Value.*

Cluster	Enrichment score	#Genes	Significance	
Annotation Cluster 1	Enrichment Score: 3.08	Count	*p*-Value	Benjamini
	Apoptosis & ER Stress	6	1.10E-05	6.40E-03
Annotation Cluster 2	Enrichment Score: 1.72	Count	*p*-Value	Benjamini
	BRLZ, Negative Regulation of Transcription	6	2.10E-06	4.20E-04
Annotation Cluster 3	Enrichment Score: 1.09	Count	*p*-Value	Benjamini
	Protein - Tyrosine Phosphatase	3	2.50E-02	1.00E+00
Annotation Cluster 4	Enrichment Score: 0.86	Count	*p*-Value	Benjamini
	GTPase Activator	4	9.30E-02	1.00E+00

Table III. *Unique DEGs in the LDH-A/B DKO vs. LDH-A/B DKO + MPP. The data are expressed as Gene symbol, FC, and p-Value.*

Gene Symbol	Description	Fold change	*p*-Value	FDR *p*-Value
AGPAT5	1-acylglycerol-3-phosphate O-acyltransferase 5	2.18	1.07E-05	8.00E-04
DHCR24	24-dehydrocholesterol reductase	–2.14	1.17E-05	9.00E-04
DHCR7	7-dehydrocholesterol reductase	–2.14	5.01E-05	2.30E-03
ACAT2	Acetyl-CoA acetyltransferase 2	–2.56	2.44E-06	3.00E-04
ACAA2	Acetyl-CoA acyltransferase 2	–3.05	4.60E-07	1.00E-04
ASCL2	Achaete-scute family bHLH transcription factor 2	–3.24	1.14E-05	9.00E-04
ACAD9	Acyl-CoA dehydrogenase family, member 9	–2.06	1.77E-05	1.20E-03
ACADSB	Acyl-CoA dehydrogenase, short/branched chain	–2.23	1.43E-05	1.00E-03
AHNAK2	AHNAK nucleoprotein 2	5.27	2.34E-07	9.47E-05
AARS	Alanyl-tRNA synthetase	3.05	5.00E-04	1.04E-02
ALDH1B1	Aldehyde dehydrogenase 1 family, member B1	–4.63	6.25E-08	4.07E-05
ALDH18A1	Aldehyde dehydrogenase 18 family, member A1	–2.18	1.24E-05	9.00E-04
ALDH3A1	Aldehyde dehydrogenase 3 family, member A1	–2.84	5.10E-03	5.75E-02
AKR1C3	Aldo-keto reductase family 1, member C3	–2.2	5.00E-04	1.14E-02
ASB4	Ankyrin repeat and SOCS box containing 4	–2.97	5.06E-08	3.59E-05
ARMC3	Armadillo repeat containing 3	–3.61	1.00E-04	4.30E-03
ARRDC3	Arrestin domain containing 3	4.55	8.25E-07	2.00E-04
ATP5D	ATP synthase, H+ transporting, mitochondrial F1 complex, delta subunit	–2.05	5.42E-06	5.00E-04
BAAT	Bile acid-CoA:amino acid N-acyltransferase	–3.44	5.29E-07	1.00E-04
CRAT	Carnitine O-acetyltransferase	–2.07	2.01E-05	1.20E-03
CPT1C	Carnitine palmitoyltransferase 1C	–2.11	5.05E-06	5.00E-04
CPT2	Carnitine palmitoyltransferase 2	–2.16	1.12E-06	2.00E-04
CASP5	Caspase 5	6.98	6.10E-10	3.27E-06
CEMIP	Cell migration inducing protein, hyaluronan binding	–3.02	6.25E-09	1.08E-05
CRBN	Cereblon	2.57	4.28E-08	3.33E-05
CFAP126	Cilia and flagella associated protein 126	–7.14	4.06E-07	1.00E-04
CKB	Creatine kinase, brain	–2.95	1.59E-05	1.10E-03
CDK1	Cyclin-dependent kinase 1	–3.15	2.18E-06	3.00E-04
CPEB3	Cytoplasmic polyadenylation element binding protein 3	3.06	3.13E-06	4.00E-04
DAGLA	Diacylglycerol lipase, alpha	2.16	1.50E-03	2.46E-02
ERN1	Endoplasmic reticulum to nucleus signaling 1	3.03	2.47E-05	1.40E-03
FAM171B	Family with sequence similarity 171, member B	–3.56	1.92E-09	5.78E-06
FAM216A	Family with sequence similarity 216, member A	–2.56	4.92E-08	3.55E-05
FADS1	Fatty acid desaturase 1	–2.25	4.34E-06	5.00E-04
FASN	Fatty acid synthase	–2.16	2.75E-05	1.50E-03
GMNN	Geminin, DNA replication inhibitor	–3.06	1.29E-06	2.00E-04
GPAT3	Glycerol-3-phosphate acyltransferase 3	2.08	2.43E-05	1.40E-03
GMPR	Guanosine monophosphate reductase	–4.18	5.00E-04	1.14E-02
HKDC1	Hexokinase domain containing 1	3.72	2.40E-03	3.41E-02
HIST2H2AA4; HIST2H2AA3	Histone cluster 2, H2aa4; histone cluster 2, H2aa3	–3.67	1.69E-08	2.02E-05
HIST2H2BB; HIST2H3PS2	Histone cluster 2, H2bb (pseudogene); histone cluster 2, H3, pseudogene 2	–4.6	6.06E-08	4.07E-05
ID3	Inhibitor of DNA binding 3, dominant negative helix-loop-helix protein	–2.74	1.73E-07	7.92E-05
IFITM3	Interferon induced transmembrane protein 3	–3.63	5.73E-09	1.08E-05
IDH2	Isocitrate dehydrogenase 2 (NADP+), mitochondrial	–2.61	9.89E-07	2.00E-04
KRT75	Keratin 75, type II	8.05	4.52E-10	3.22E-06
LEMD1; BLACAT1	LEM domain containing 1; bladder cancer associated transcript 1 (non-protein coding)	3.11	1.77E-07	7.94E-05
LINC01207	Long intergenic non-protein coding RNA 1207	3.8	3.53E-07	1.00E-04
MME	Membrane metallo-endopeptidase	–3.25	6.04E-06	6.00E-04
MT1H	Metallothionein 1H	–3.18	6.01E-05	2.60E-03
MIR1244-1; MIR1244-2; MIR1244-3; MIR1244-4	MicroRNA 1244-1; microRNA 1244-2; microRNA 1244-3; microRNA 1244-4	–3.74	6.75E-07	2.00E-04
MSN	Moesin	2.53	3.89E-08	3.29E-05
NEDD4L	Neural precursor cell expressed, developmentally down-regulated 4-like, E3 ubiquitin protein ligase	3.31	5.95E-09	1.08E-05
NTS	Neurotensin	–5.78	8.02E-06	7.00E-04
NID1	Nidogen 1	4.77	2.58E-07	9.92E-05

Table III. *Continued*

Table III. *Continued*

Gene Symbol	Description	Fold change	*p*-Value	FDR *p*-Value
NDRG1	N-myc downstream regulated 1	3.64	2.60E-03	3.63E-02
PLCB4	Phospholipase C, beta 4	–3.09	8.76E-07	2.00E-04
PEA15	Phosphoprotein enriched in astrocytes 15	2.34	1.10E-07	6.18E-05
PRTFDC1	Phosphoribosyl transferase domain containing 1	–3.17	1.97E-07	8.43E-05
PIWIL1	Piwi-like RNA-mediated gene silencing 1	–4.49	1.52E-08	1.94E-05
PLLP	Plasmolipin	–3.48	4.16E-08	3.29E-05
PDK3	Pyruvate dehydrogenase kinase, isozyme 3	–2.09	2.00E-04	5.90E-03
PDP1	Pyruvate dehyrogenase phosphatase catalytic subunit 1	2.54	1.78E-07	7.94E-05
REEP6	Receptor accessory protein 6	–4.56	3.11E-10	3.00E-06
RNASEL	Ribonuclease L (2,5-oligoisoadenylate synthetase-dependent)	3.42	4.45E-06	5.00E-04
RRM2	Ribonucleotide reductase M2	–6.31	5.15E-10	3.22E-06
RNF144A	Ring finger protein 144A	3.68	8.72E-07	2.00E-04
RNU5D-1	RNA, U5D small nuclear 1	–10.92	1.60E-07	7.50E-05
RNU5F-1	RNA, U5F small nuclear 1	–6.38	9.97E-06	8.00E-04
SAMHD1	SAM domain and HD domain 1	–3.97	7.19E-09	1.20E-05
SLFN5	Schlafen family member 5	7.24	2.81E-06	3.00E-04
SNORA11; MAGED2	Small nucleolar RNA, H/ACA box 11; MAGE family member D2	4.17	3.40E-05	1.80E-03
SLC12A2	Solute carrier family 12 (sodium/potassium/chloride transporter), member 2	–4.32	9.46E-10	4.52E-06
SLC22A15	Solute carrier family 22, member 15	4.07	4.00E-04	9.40E-03
SLC25A37	Solute carrier family 25 (mitochondrial iron transporter), member 37	2.54	1.24E-07	6.62E-05
SRM	Spermidine synthase	–3.02	6.31E-06	6.00E-04
SOAT1	sterol O-acyltransferase 1	–2.87	6.49E-06	6.00E-04
SOD2	Superoxide dismutase 2, mitochondrial	–2.25	1.30E-03	2.25E-02
TESC	Tescalcin	–3	3.12E-07	1.00E-04
TK1	Thymidine kinase 1, soluble	–3.12	2.96E-06	4.00E-04
TIMELESS	Timeless circadian clock	–4.11	1.38E-08	1.86E-05
TMEM9B-AS1	TMEM9B antisense RNA 1	3.6	2.71E-06	3.00E-04
TMEM71; LRRC6	Transmembrane protein 71; leucine rich repeat containing 6	3.11	1.07E-07	6.07E-05
UBE2T	Ubiquitin conjugating enzyme E2T	–3.74	5.18E-09	1.08E-05
USP18	Ubiquitin specific peptidase 18	–3	9.39E-07	2.00E-04
XDH	Xanthine dehydrogenase	3.25	1.36E-07	6.92E-05
ZC3H6	Zinc finger CCCH-type containing 6	3.33	6.59E-06	6.00E-04
ZNF25	Zinc finger protein 25	3.22	5.63E-06	5.00E-04
ZNF555	Zinc finger protein 555	6.76	6.40E-08	4.07E-05

having no capacity to produce lactic acid or drive the alternative ATP SLP pathway. We expected to see complete energy collapse in the LDH-A/B DKO, as reported by others combining mitochondrial inhibitors with glycolytic inhibitors such as DG this was not the case (70, 74-76). Keep in mind, this is a unique model, where glycolysis is still functioning to the point of pyruvic acid, so in the true sense, the LDH-A/BDKO is not a full glycolytic inhibitor but does effectively shut down the required pyruvate to lactate conversion sustain the anaerobic production of ATP through SLP. The data from this study show an unexpected resistance to the toxin in the LDH-A/B DKO, which requires further explanation.

The data in this work establish efficacy of MPP+ to inhibit mitochondrial function, both biologically through suppressive respiration and an observed transcriptional loss of OXPHOS of complex I; NADH dehydrogenase, subunits 3, and 6 and complex III (cytochrome b). Moreover, the data in this work support our previous study in that the LDHA/B-DKO cell line triggered a metabolic response with heightened OXPHOS capacity (15). The baseline respiratory differential may have contributed to a resistance to MPP+ either by necessitating a higher required concentration of MPP+ to elicit damage, or possibly by extruding the drug equipped with high capacity ATPase multi-drug resistance pumps, as there is a clear relationship between higher OXPHOS stem cell metabolism, chemo-resistance, enhanced expression of ATP binding cassette multi-drug resistance pumps and poor clinical outcomes (77-79).

Some of the changes that accompany this resistance are reflected in the transcriptome when analyzing the differential between CV *vs*. CV + MPP+ and LDH-A/B DKO *vs*. LDH-A/B DKO + MPP+, such as heightened ATP binding cassette subfamily C member 3 (ABCC3) multi-drug resistance pump and a differential in the flow of intermediates from pyruvate (glycolysis) to Acetyl-CoA (TCA) or *vice versa*. MPP+ in

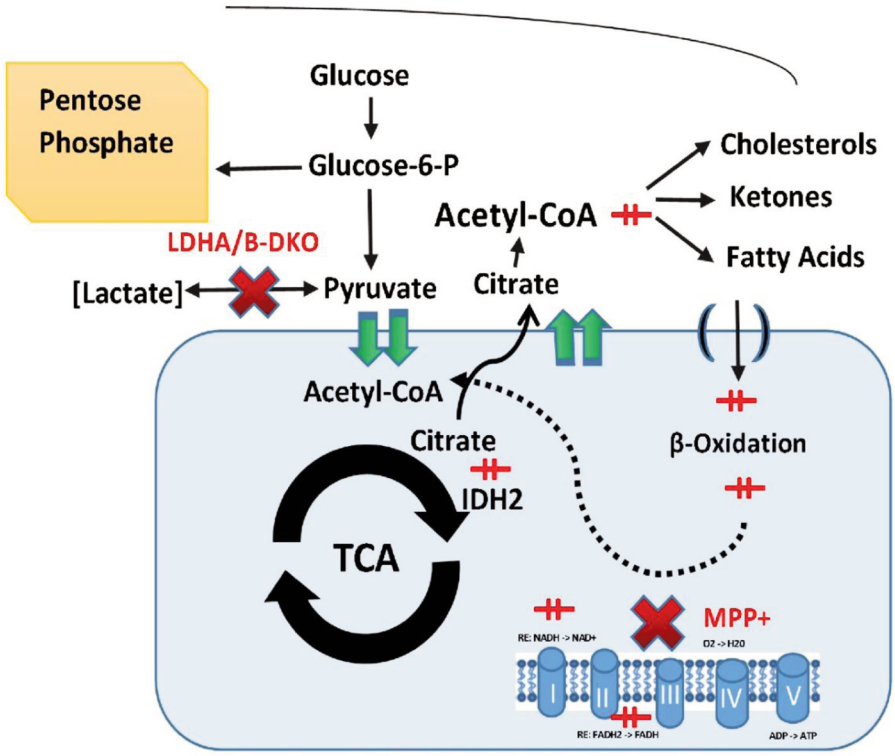

Figure 11. *Effects of MPP+ in the LDH-A/B DKO cell line. In brief, SLP was compromised by genetic editing of LDH-A/B which blocked production of lactic acid. Chemical challenge to the mitochondria was established using MPP+, effective in attenuating cell respiration and transcriptionally Complex I-V related elements. In the LDH-A/B DKO, we see an elevation in transcripts that allow greater flow of pyruvate to the mitochondria and conversion to acetyl-CoA through the pyruvate dehydrogenase complex. There was a pull back down-regulation on inhibitory kinase controls (PDK3) and an up-regulation on forward phosphatase controls (PDP1). The transcriptome showed a down-regulation of iso-citrate dehydrogenase (mitochondrial) required for the tricarboxylic acid (TCA) cycle and enzymes involved with the transport and oxidation of fatty acids: entry of (CPT1C, CPT2), initial steps in (ACAD9, ACADSB) and final steps required for the B-oxidation spiral (ACAA 2). Lower electron transport chain activity, coincided with lower expression of genes (TCA and fatty acid oxidation) which would generate equivalents (NADH and FADH2) , no longer being accepted to generate an electrochemical gradient for ATP production. In addition, acetyl-CoA which is the central carbon currency to fuel energy related processes is also met with a down-regulation of its route through biosynthetic processes including: down-regulated transcripts required for the initiation step of cholesterol/ ketone synthesis (ACAT2), the final step of cholesterol synthesis (DHCR 7, DHCR 24) and fatty acid synthesis (FAS).*

the CV resulted in a unique (CV set only) elevation of phosphoenolpyruvate carboxykinase 1 (PKC1), indicative of a response to nutrient deprivation (80) with capacity to redirect carbons from oxaloacetate back into glycolysis to carry out gluconeogenesis. In contrast, the LDH-A/B DKO exposed to MPP+ responded with up-regulation of positive regulator of pyruvate dehydrogenase (PDH), PDH phosphatase catalytic subunit 1 (PDP1) with a down-regulation of negative PDH feedback; PDH kinase, isozyme 3 (PDK3), effect that would push pyruvate to enter the mitochondria, and its conversion to acetyl-CoA. While the LDH-A/B DKO MPP+ treatment group show greater pyruvate to Acetyl-CoA production while there is no conversion of pyruvate to lactic acid, the transcriptome suggests a pooling or accumulation of Acetyl-CoA, since these changes coincide with a reduction in transcripts that code for proteins which enable Acetyl-CoA to be used to drive biosynthetic processes (fatty acid, cholesterol and ketone synthesis).

Examples of these include specific losses in the LDH-A/B DKO MPP+ group (not in the CV + MPP+ group), including down-regulation of 1) acyl-CoA dehydrogenase (ACAD9, ACADSB) (initial steps in the fatty acid β-oxidation pathway) 2) acetyl-CoA acyltransferase 2 (ACAA2) (final steps of the fatty acid beta-oxidation pathway) 3), carnitine palmitoyltransferase (CPT1C, CPT2) (entry of fatty acids into the mitochondria) and 4) isocitrate dehydrogenase (mitochondrial) iso-citrate dehydrogenase 2 (IDH2) which would be required for acetyl-CoA metabolism to drive the TCA cycle. These changes are logically and biochemical sound since a hampered ETC by MPP+ would abate proton shuttling. Therefore, losses in enzymes that drive TCA and

FA beta-oxidation pathways would also be reduced since the mitochondria no longer accept reducing equivalents (NADH and FADH2) from these pathways to generate an electrochemical gradient for ATP production (9).

The pooling of acetyl-CoA seems to be a unique central aspect in the LDH-A/B DKOs + MPP+ (not present in the CV *vs*. CV + MPP+), as there is also a loss of transcripts that encode proteins required to carry out anabolic substrate use of acetyl-CoA to produce cholesterols, fatty acids, and ketones. These include losses to 1) acetyl-CoA acetyltransferase 2) (ACAT2) (the first enzyme in the cholesterol and ketone synthesis pathway which is required to convert two molecules of acetyl-CoA to acetoacetyl-CoA), 2) the final step for cholesterol biosynthesis 24-dehydrocholesterol reductase, 7 dehydrocholesterol reductase (DHCR 7 & 24) and 3) reduction of fatty acid synthase (FAS) needed to carry out condensation reactions from acetyl-CoA and malonyl-CoA and a corresponding loss to fatty acid desaturase 1 (which catalyzes the removal of two hydrogen atoms from a fatty acid, creating a carbon/carbon double bond). These changes coincided with an increase in glycerol-3-phosphate (GPAT3) O-acyltransferase which catalyzes the chemical reaction where by acyl-CoA + sn-glycerol 3-phosphate is converted to CoA + 1-acyl-sn-glycerol 3-phosphate required for the organization of phospholipids to sustain biological membrane structures. Acetyl-CoA is the central carbon currency of energy metabolism. It is synthesized from pyruvate in mitochondria, enters into the TCA cycle for conversion to citric acid cycle (citrate synthase), and excess citrate is exported to the cytoplasm by a mitochondrial citrate carrier, where it is reconverted back to acetyl-CoA by ATP-citrate lyase (ACLY) then available for fatty acid, ketone, cholesterol synthesis or acetylation reactions that involve both protein and epigenetic cellular function including histone and chromatin remodeling, which controls transcription of mRNA (81, 82). The central functional role of ACLY in driving lipid catabolic tumorigenic processes is the rationale behind the development of inhibitors (*e.g*., hydroxycitrate, bempedoic acid) in oncology research (83, 84). Clearly, acetyl-CoA has a central role in cancer metabolism and also essential to carrying out epigenetic histone modifications/ lysine acetylation (85). Future studies will be required to examine how acetyl-CoA is being utilized in the absence of a functional glycolytic pathway, why it is accruing and how it is being used.

The transcriptome data also reflects the importance of epigenetic changes elicited by MPP+ in both CV and LDH-A/B DKOs, evidenced by the sheer number of down-regulated histone cluster transcripts as well as the massive bidirectional DEGs in non-protein coding microRNA and long-intergenic transcripts. MPP+ also evoked changes in a number of METTL transcripts, which are believed to contribute to nucleoside modifications in diverse types of RNA and DNA (86, 87), however very little is known on these particular epigenetic modifications.

MPP+ and cell cycle. Other than a loss of OXPHOS by MPP+ as anticipated (88, 89) the most significant effect to both groups was a loss of transcripts otherwise required for cell cycle. In both groups we the MPP+ mediated down-regulation of cell cycle genes (CDC20, CDC25A, CDC25C, CDC45, CDC6, CDC 7), cell cycle associated genes (CDCA2, CDCA3, CDCA7 and CDCA8), cyclins (cyclin A2, B1, B2, D, D2, E1, E2, F, L1), cyclin-dependent kinases (CDK1, CDK13, CDK14) and marker of proliferation Ki-67 (MIK67). The effects of MPP+ on both cell lines also resulted in down-regulation of DNA replicative processes including the following: mini-chromosome maintenance complex components (MCMs 2, 3, 4, 5, 6, 7, 8, 9, 10) origin recognition complex subunits (ORCs 1, 2, 5, 6), kinesin family member genes (KIFs 11, 14, 15, 18A, 20A, 20B, 23, 4A) centromere proteins (CENPE E, F, H, I, J, K, M, N, O, P, Q, U, W) and centrosomal proteins of kDa (128 kDa, 135 kDa, 152 kDa, 162 kDa, 192 kDa, 19 kDa, 295 kDa, 55 kDa, 76 kDa, 78 kDa, 83 kDa and 97 kDa). Down-regulation also extended to loss of transcripts required replicative DNA processes including; DNA polymerases (POLs A1, A2, D2, E2, Q, D4), DNA primases (PRIMs 1 and 2), DNA repair transcripts (DNA crosslink repair genes: DCLREs 1A,1B and 1C), DNA replication helicase/nuclease gene 2i; GINS complex subunits (Psf1 homolog) (GINS 1, 2, 3 and 4); Fanconi anemia complementation group (FANC A, B, C, D2, I, L and M); spindle and kinetochore associated complex subunits (SKA1,3) and topoisomerases (TOPs 2A, 2B, 2C). These findings are in alignment with others showing the effects of MPP+ in vitro in exerting cytostatic effects, secondary to cell death initiated by glucose depletion as a result of accelerated glycolysis (88, 90). Whatever the consequence, there is no doubt that MPP+ caused a significant amount of stress on both cell lines, reflected by up-regulation of DNA-damage-inducible, alpha (CADD45A) beta (GADD45B) gamma (GADD45H), commonly the aftermath of strain associated with the loss of cell cycle progression (91) particularly inability to pass the G2-M phase (92-94). Refer to the data located in NIH Gene Expression Omnibus at https://www.ncbi.nlm.nih.gov/geo/query/acc.cgi?acc=GSE149289.

Conclusion

The findings from this study suggest a complex metabolic survival response to a specific mitochondrial toxin (MPP+) in colon cancer cells that lack LDH-A/B transcripts and the related functional SLP glycolytic anaerobic ATP energy yielding pathway. While this study provides a framework for further analysis, cancer cells without LDH may shift toward aerobic OXPHOS creating counter indication when using mitochondrial targeting drugs, which may necessitate higher concentration.

Availability of Data and Material

The dataset has been deposited to NIH Gene Expression Omnibus located at https://www.ncbi.nlm.nih.gov/geo/query/acc.cgi?acc=GSE149289.

Conflicts of Interest

The Authors declare that they have no conflicts of interest.

Authors' Contributions

NM conducted studies on basic cell metabolic profiles. EM assisted with these studies and carried out microarray work. RB was involved with mechanistic troubleshooting and study design and KS oversaw and guided this project.

Acknowledgments

This research was supported by the National Institute of Minority Health and Health Disparities of the National Institutes of Health through Grant Number U54 MD007582 and Grant Number P20 MD006738. We are very grateful for the work of Dr. J Pouyssegur, Dr. S. Cassim, and Dr. M Zdralevic from the University Cote d'Azur, IRCAN, CNRS, Centre A. Lacassagne, Nice, France and Department of Medical Biology, Centre Scientifique de Monaco, Monaco and their generosity in establishing and contributing these cell lines.

References

1 Zam W, Ahmed I and Yousef H: Warburg effects on cancer cells survival: the role of sugar starvation in cancer therapy. Curr Clin Pharmacol, 2020. PMID: 32282309. DOI: 10.2174/1574884715666200413121756

2 Bayley JP and Devilee P: Warburg tumours and the mechanisms of mitochondrial tumour suppressor genes. Barking up the right tree? Curr Opin Genet Dev *20(3)*: 324-329, 2010. PMID: 20304625. DOI: 10.1016/j.gde.2010.02.008

3 Zhao B, Luo J, Yu T, Zhou L, Lv H and Shang P: Anticancer mechanisms of metformin: A review of the current evidence. Life Sci *254*: 117717, 2020. PMID: 32339541. DOI: 10.1016/j.lfs.2020.117717

4 Oshima N, Ishida R, Kishimoto S, Beebe K, Brender JR, Yamamoto K, Urban D, Rai G, Johnson MS, Benavides G, Squadrito GL, Crooks D, Jackson J, Joshi A, Mott BT, Shrimp JH, Moses MA, Lee MJ, Yuno A, Lee TD, Hu X, Anderson T, Kusewitt D, Hathaway HH, Jadhav A, Picard D, Trepel JB, Mitchell JB, Stott GM, Moore W, Simeonov A, Sklar LA, Norenberg JP, Linehan WM, Maloney DJ, Dang CV, Waterson AG, Hall M, Darley-Usmar VM, Krishna MC and Neckers LM: Dynamic imaging of LDH inhibition in tumors reveals rapid *in vivo* metabolic rewiring and vulnerability to combination therapy. Cell Rep *30(6)*: 1798-1810.e4, 2020. PMID: 32049011. DOI: 10.1016/j.celrep.2020.01.039

5 Zhou Y, Tao P, Wang M, Xu P, Lu W, Lei P and You Q: Development of novel human lactate dehydrogenase A inhibitors: High-throughput screening, synthesis, and biological evaluations. Eur J Med Chem *177*: 105-115, 2019. PMID: 31129449. DOI: 10.1016/j.ejmech.2019.05.033

6 Kim B, Jung JW, Jung J, Han Y, Suh DH, Kim HS, Dhanasekaran DN and Song YS: PGC1α induced by reactive oxygen species contributes to chemoresistance of ovarian cancer cells. Oncotarget *8(36)*: 60299-60311, 2017. PMID: 28947972. DOI: 10.18632/oncotarget.19140

7 Praharaj PP, Patro BS and Bhutia SK: Dysregulation of mitophagy and mitochondrial homeostasis in cancer stem cells: Novel mechanism for anti-cancer stem cell-targeted cancer therapy. Br J Pharmacol, 2021. PMID: 33527371. DOI: 10.1111/bph.15401

8 Praharaj PP, Panigrahi DP, Bhol CS, Patra S, Mishra SR, Mahapatra KK, Behera BP, Singh A, Patil S and Bhutia SK: Mitochondrial rewiring through mitophagy and mitochondrial biogenesis in cancer stem cells: A potential target for anti-CSC cancer therapy. Cancer Lett *498*: 217-228, 2021. PMID: 33186655. DOI: 10.1016/j.canlet.2020.10.036

9 Grasso D, Zampieri LX, Capelôa T, Van de Velde JA and Sonveaux P: Mitochondria in cancer. Cell Stress *4(6)*: 114-146, 2020. PMID: 32548570. DOI: 10.15698/cst2020.06.221

10 Wei Z, Jia J, Heng G, Xu H, Shan J, Wang G, Liu C, Xia J, Zhou H, Wu M, Yang Z, Wang M, Xiong Z, Huang H, Liu L and Qian C: Sirtuin-1/Mitochondrial ribosomal protein S5 axis enhances the metabolic flexibility of liver cancer stem cells. Hepatology *70(4)*: 1197-1213, 2019. PMID: 30901096. DOI: 10.1002/hep.30622

11 Mack N, Mazzio EA, Bauer D, Flores-Rozas H and Soliman KF: Stable shRNA silencing of lactate dehydrogenase A (LDHA) in human MDA-MB-231 breast cancer cells fails to alter lactic acid production, glycolytic activity, ATP or survival. Anticancer Res *37(3)*: 1205-1212, 2017. PMID: 28314283. DOI: 10.21873/anticanres.11435

12 Deiab S, Mazzio E, Messeha S, Mack N and Soliman KF: High-throughput screening to identify plant derived human LDH-A inhibitors. European J Med Plants *3(4)*: 603-615, 2013. PMID: 24478981. DOI: 10.9734/ejmp/2013/5995

13 Deiab S, Mazzio E, Eyunni S, McTier O, Mateeva N, Elshami F and Soliman KF: 1,2,3,4,6-Penta-O-galloylglucose within galla chinensis inhibits human LDH-A and attenuates cell proliferation in MDA-MB-231 breast cancer cells. Evid Based Complement Alternat Med *2015*: 276946, 2015. PMID: 25918543. DOI: 10.1155/2015/276946

14 Ždralević M, Brand A, Di Ianni L, Dettmer K, Reinders J, Singer K, Peter K, Schnell A, Bruss C, Decking SM, Koehl G, Felipe-Abrio B, Durivault J, Bayer P, Evangelista M, O'Brien T, Oefner PJ, Renner K, Pouysségur J and Kreutz M: Double genetic disruption of lactate dehydrogenases A and B is required to ablate the "Warburg effect" restricting tumor growth to oxidative metabolism. J Biol Chem *293(41)*: 15947-15961, 2018. PMID: 30158244. DOI: 10.1074/jbc.RA118.004180

15 Mazzio E, Badisa R, Mack N, Cassim S, Zdralevic M, Pouyssegur J and Soliman KFA: Whole-transcriptome analysis of fully viable energy efficient glycolytic-null cancer cells established by double genetic knockout of lactate dehydrogenase A/B or glucose-6-phosphate isomerase. Cancer Genomics Proteomics *17(5)*: 469-497, 2020. PMID: 32859627. DOI: 10.21873/cgp.20205

16 Yu D, Liu C and Guo L: Mitochondrial metabolism and cancer metastasis. Ann Transl Med *8(14)*: 904, 2020. PMID: 32793748. DOI: 10.21037/atm.2020.03.42

17 Yoshida GJ: Beyond the Warburg Effect: N-Myc Contributes to metabolic reprogramming in cancer cells. Front Oncol *10*: 791, 2020. PMID: 32547946. DOI: 10.3389/fonc.2020.00791

18 Oliveira GL, Coelho AR, Marques R and Oliveira PJ: Cancer cell metabolism: Rewiring the mitochondrial hub. Biochim Biophys Acta Mol Basis Dis *1867(2)*: 166016, 2021. PMID: 33246010. DOI: 10.1016/j.bbadis.2020.166016
19 McCann E, O'Sullivan J and Marcone S: Targeting cancer-cell mitochondria and metabolism to improve radiotherapy response. Transl Oncol *14(1)*: 100905, 2021. PMID: 33069104. DOI: 10.1016/j.tranon.2020.100905
20 Sica V, Bravo-San Pedro JM, Stoll G and Kroemer G: Oxidative phosphorylation as a potential therapeutic target for cancer therapy. Int J Cancer *146(1)*: 10-17, 2020. PMID: 31396957. DOI: 10.1002/ijc.32616
21 Varela-López A, Vera-Ramírez L, Giampieri F, Navarro-Hortal MD, Forbes-Hernández TY, Battino M and Quiles JL: The central role of mitochondria in the relationship between dietary lipids and cancer progression. Semin Cancer Biol : , 2021. PMID: 33434641. DOI: 10.1016/j.semcancer.2021.01.001
22 Nagarajan SR, Butler LM and Hoy AJ: The diversity and breadth of cancer cell fatty acid metabolism. Cancer Metab *9(1)*: 2, 2021. PMID: 33413672. DOI: 10.1186/s40170-020-00237-2
23 Reyes-Castellanos G, Masoud R and Carrier A: Mitochondrial metabolism in PDAC: From better knowledge to new targeting strategies. Biomedicines *8(8)*, 2020. PMID: 32756381. DOI: 10.3390/biomedicines8080270
24 Vasan K, Werner M and Chandel NS: Mitochondrial metabolism as a target for cancer therapy. Cell Metab *32(3)*: 341-352, 2020. PMID: 32668195. DOI: 10.1016/j.cmet.2020.06.019
25 Sica V, Bravo-San Pedro JM, Izzo V, Pol J, Pierredon S, Enot D, Durand S, Bossut N, Chery A, Souquere S, Pierron G, Vartholomaiou E, Zamzami N, Soussi T, Sauvat A, Mondragón L, Kepp O, Galluzzi L, Martinou JC, Hess-Stumpp H, Ziegelbauer K, Kroemer G and Maiuri MC: Lethal poisoning of cancer cells by respiratory chain inhibition plus Dimethyl α-Ketoglutarate. Cell Rep *27(3)*: 820-834.e9, 2019. PMID: 30995479. DOI: 10.1016/j.celrep.2019.03.058
26 McMillian MK, Li L, Parker JB, Patel L, Zhong Z, Gunnett JW, Powers WJ and Johnson MD: An improved resazurin-based cytotoxicity assay for hepatic cells. Cell Biol Toxicol *18(3)*: 157-173, 2002. PMID: 12083422. DOI: 10.1023/a:1015559603643
27 Szklarczyk D, Franceschini A, Kuhn M, Simonovic M, Roth A, Minguez P, Doerks T, Stark M, Muller J, Bork P, Jensen LJ and von Mering C: The STRING database in 2011: functional interaction networks of proteins, globally integrated and scored. Nucleic Acids Res *39(Database issue)*: D561-D568, 2011. PMID: 21045058. DOI: 10.1093/nar/gkq973
28 Szklarczyk D, Gable AL, Nastou KC, Lyon D, Kirsch R, Pyysalo S, Doncheva NT, Legeay M, Fang T, Bork P, Jensen LJ and von Mering C: The STRING database in 2021: customizable protein-protein networks, and functional characterization of user-uploaded gene/measurement sets. Nucleic Acids Res *49(D1)*: D605-D612, 2021. PMID: 33237311. DOI: 10.1093/nar/gkaa1074
29 Huang DW, Sherman BT, Tan Q, Collins JR, Alvord WG, Roayaei J, Stephens R, Baseler MW, Lane HC and Lempicki RA: The DAVID Gene Functional Classification Tool: a novel biological module-centric algorithm to functionally analyze large gene lists. Genome Biol *8(9)*: R183, 2007. PMID: 17784955. DOI: 10.1186/gb-2007-8-9-r183
30 Mazzio EA, Smith B and Soliman KF: Evaluation of endogenous acidic metabolic products associated with carbohydrate metabolism in tumor cells. Cell Biol Toxicol *26(3)*: 177-188, 2010. PMID: 19784859. DOI: 10.1007/s10565-009-9138-6
31 Bao X, Zhang J, Huang G, Yan J, Xu C, Dou Z, Sun C and Zhang H: The crosstalk between HIFs and mitochondrial dysfunctions in cancer development. Cell Death Dis *12(2)*: 215, 2021. PMID: 33637686. DOI: 10.1038/s41419-021-03505-1
32 Cuezva JM, Krajewska M, de Heredia ML, Krajewski S, Santamaría G, Kim H, Zapata JM, Marusawa H, Chamorro M and Reed JC: The bioenergetic signature of cancer: a marker of tumor progression. Cancer Res *62(22)*: 6674-6681, 2002. PMID: 12438266
33 Mazzio EA, Boukli N, Rivera N and Soliman KF: Pericellular pH homeostasis is a primary function of the Warburg effect: inversion of metabolic systems to control lactate steady state in tumor cells. Cancer Sci *103(3)*: 422-432, 2012. PMID: 22320183. DOI: 10.1111/j.1349-7006.2012.02206.x
34 Burgdorf S, Porubsky S, Marx A and Popovic ZV: Cancer acidity and hypertonicity contribute to dysfunction of tumor-associated dendritic cells: Potential impact on antigen cross-presentation machinery. Cancers (Basel) *12(9)*, 2020. PMID: 32847079. DOI: 10.3390/cancers12092403
35 Lebelo MT, Joubert AM and Visagie MH: Warburg effect and its role in tumourigenesis. Arch Pharm Res *42(10)*: 833-847, 2019. PMID: 31473944. DOI: 10.1007/s12272-019-01185-2
36 Hamaguchi R, Ito T, Narui R, Morikawa H, Uemoto S and Wada H: Effects of alkalization therapy on chemotherapy outcomes in advanced pancreatic cancer: A retrospective case-control study. In Vivo *34(5)*: 2623-2629, 2020. PMID: 32871792. DOI: 10.21873/invivo.12080
37 Ando H, Eshima K and Ishida T: Neutralization of acidic tumor microenvironment (TME) with daily oral dosing of sodium potassium citrate (K/Na Citrate) increases therapeutic effect of anti-cancer agent in pancreatic cancer xenograft mice model. Biol Pharm Bull *44(2)*: 266-270, 2021. PMID: 33518679. DOI: 10.1248/bpb.b20-00825
38 Abdel-Wahab AF, Mahmoud W and Al-Harizy RM: Targeting glucose metabolism to suppress cancer progression: prospective of anti-glycolytic cancer therapy. Pharmacol Res *150*: 104511, 2019. PMID: 31678210. DOI: 10.1016/j.phrs.2019.104511
39 Onyango IG, Khan SM and Bennett JP Jr: Mitochondria in the pathophysiology of Alzheimer's and Parkinson's diseases. Front Biosci (Landmark Ed) *22*: 854-872, 2017. PMID: 27814651. DOI: 10.2741/4521
40 McKnight S and Hack N: Toxin-Induced parkinsonism. Neurol Clin *38(4)*: 853-865, 2020. PMID: 33040865. DOI: 10.1016/j.ncl.2020.08.003
41 Xu Y, Pan S, Jiang W, Xue F and Zhu X: Effects of propofol on the development of cancer in humans. Cell Prolif *53(8)*: e12867, 2020. PMID: 32596964. DOI: 10.1111/cpr.12867
42 Lotz C, Stumpner J and Smul TM: Sevoflurane as opposed to propofol anesthesia preserves mitochondrial function and alleviates myocardial ischemia/reperfusion injury. Biomed Pharmacother *129*: 110417, 2020. PMID: 32574972. DOI: 10.1016/j.biopha.2020.110417
43 Qin J, Li Y and Wang K: Propofol induces impairment of mitochondrial biogenesis through inhibiting the expression of peroxisome proliferator-activated receptor-γ coactivator-1α. J Cell Biochem *120(10)*: 18288-18297, 2019. PMID: 31190345. DOI: 10.1002/jcb.29138
44 Sumi C, Okamoto A, Tanaka H, Nishi K, Kusunoki M, Shoji T, Uba T, Matsuo Y, Adachi T, Hayashi JI, Takenaga K and Hirota

K: Propofol induces a metabolic switch to glycolysis and cell death in a mitochondrial electron transport chain-dependent manner. PLoS One *13(2)*: e0192796, 2018. PMID: 29447230. DOI: 10.1371/journal.pone.0192796

45 Zhu G, Zhang L, Dan J and Zhu Q: Differential effects and mechanisms of local anesthetics on esophageal carcinoma cell migration, growth, survival and chemosensitivity. BMC Anesthesiol *20(1)*: 126, 2020. PMID: 32450791. DOI: 10.1186/s12871-020-01039-1

46 Zhu Q, Zhu G, Xu W, Dan J, Xia R and Liu W: Bupivacaine inhibits angiogenesis through oxidative stress-dependent inhibition of Akt/mTOR and activation of AMPK. Fundam Clin Pharmacol *34(5)*: 581-590, 2020. PMID: 32145095. DOI: 10.1111/fcp.12554

47 Yang J, Li G, Bao K, Liu W, Zhang Y and Ting W: Ropivacaine inhibits tumor angiogenesis *via* sodium-channel-independent mitochondrial dysfunction and oxidative stress. J Bioenerg Biomembr *51(3)*: 231-238, 2019. PMID: 30847691. DOI: 10.1007/s10863-019-09793-9

48 Liu L, Qi L, Knifley T, Piecoro DW, Rychahou P, Liu J, Mitov MI, Martin J, Wang C, Wu J, Weiss HL, Butterfield DA, Evers BM, O'Connor KL and Chen M: S100A4 alters metabolism and promotes invasion of lung cancer cells by up-regulating mitochondrial complex I protein NDUFS2. J Biol Chem *294(18)*: 7516-7527, 2019. PMID: 30885944. DOI: 10.1074/jbc.RA118.004365

49 Fontaine E: Metformin-induced mitochondrial complex I inhibition: Facts, uncertainties, and consequences. Front Endocrinol (Lausanne) *9*: 753, 2018. PMID: 30619086. DOI: 10.3389/fendo.2018.00753

50 Izreig S, Gariepy A, Kaymak I, Bridges HR, Donayo AO, Bridon G, DeCamp LM, Kitchen-Goosen SM, Avizonis D, Sheldon RD, Laister RC, Minden MD, Johnson NA, Duchaine TF, Rudoltz MS, Yoo S, Pollak MN, Williams KS and Jones RG: Repression of LKB1 by *miR-17~92* sensitizes *MYC*-dependent lymphoma to biguanide treatment. Cell Rep Med *1(2)*: 100014, 2020. PMID: 32478334. DOI: 10.1016/j.xcrm.2020.100014

51 Pecinová A, Brázdová A, Drahota Z, Houštěk J and Mráček T: Mitochondrial targets of metformin-Are they physiologically relevant? Biofactors *45(5)*: 703-711, 2019. PMID: 31343786. DOI: 10.1002/biof.1548

52 Mengis CL: Lactic acid acidemia and phenformin. Rocky Mt Med J *61*: 39-41, 1964. PMID: 14221484

53 Kwong SC and Brubacher J: Phenformin and lactic acidosis: a case report and review. J Emerg Med *16(6)*: 881-886, 1998. PMID: 9848705. DOI: 10.1016/s0736-4679(98)00103-6

54 Wang GS and Hoyte C: Review of biguanide (Metformin) toxicity. J Intensive Care Med *34(11-12)*: 863-876, 2019. PMID: 30126348. DOI: 10.1177/0885066618793385

55 Jaidee R, Kongpetch S, Senggunprai L, Prawan A, Kukongviriyapan U and Kukongviriyapan V: Phenformin inhibits proliferation, invasion, and angiogenesis of cholangiocarcinoma cells *via* AMPK-mTOR and HIF-1A pathways. Naunyn Schmiedebergs Arch Pharmacol *393(9)*: 1681-1690, 2020. PMID: 32383028. DOI: 10.1007/s00210-020-01885-3

56 Pistoni M, Tondelli G, Gallo C, Torricelli F, Maresca A, Carelli V, Ciarrocchi A and Dallaglio K: Exploring metabolic reprogramming in melanoma *via* acquired resistance to the oxidative phosphorylation inhibitor phenformin. Melanoma Res *30(1)*: 1-13, 2020. PMID: 31116160. DOI: 10.1097/CMR.0000000000000624

57 Mathews Samuel S, Satheesh NJ, Ghosh S, Büsselberg D, Majeed Y, Ding H and Triggle CR: Treatment with a combination of metformin and 2-Deoxyglucose upregulates Thrombospondin-1 in microvascular endothelial cells: Implications in Anti-Angiogenic Cancer Therapy. Cancers (Basel) *11(11)*, 2019. PMID: 31698699. DOI: 10.3390/cancers11111737

58 Wokoun U, Hellriegel M, Emons G and Gründker C: Co-treatment of breast cancer cells with pharmacologic doses of 2-deoxy-D-glucose and metformin: Starving tumors. Oncol Rep *37(4)*: 2418-2424, 2017. PMID: 28350075. DOI: 10.3892/or.2017.5491

59 Cheng G, Zielonka J, Ouari O, Lopez M, McAllister D, Boyle K, Barrios CS, Weber JJ, Johnson BD, Hardy M, Dwinell MB and Kalyanaraman B: Mitochondria-targeted analogues of metformin exhibit enhanced antiproliferative and radiosensitizing effects in pancreatic cancer cells. Cancer Res *76(13)*: 3904-3915, 2016. PMID: 27216187. DOI: 10.1158/0008-5472.CAN-15-2534

60 Kafkova A and Trnka J: Mitochondria-targeted compounds in the treatment of cancer. Neoplasma *67(3)*: 450-460, 2020. PMID: 32122145. DOI: 10.4149/neo_2020_190725N671

61 Wang J, Li J, Xiao Y, Fu B and Qin Z: TPP-based mitocans: a potent strategy for anticancer drug design. RSC Med Chem *11(8)*: 858-875, 2020. PMID: 33479681. DOI: 10.1039/c9md00572b

62 Battogtokh G, Choi YS, Kang DS, Park SJ, Shim MS, Huh KM, Cho YY, Lee JY, Lee HS and Kang HC: Mitochondria-targeting drug conjugates for cytotoxic, anti-oxidizing and sensing purposes: current strategies and future perspectives. Acta Pharm Sin B *8(6)*: 862-880, 2018. PMID: 30505656. DOI: 10.1016/j.apsb.2018.05.006

63 Huang M, Myers CR, Wang Y and You M: Mitochondria as a novel target for cancer chemoprevention: Emergence of mitochondrial targeting agents. Cancer Prev Res (Phila) : , 2020. PMID: 33303695. DOI: 10.1158/1940-6207.CAPR-20-0425

64 Dilip A, Cheng G, Joseph J, Kunnimalaiyaan S, Kalyanaraman B, Kunnimalaiyaan M and Gamblin TC: Mitochondria-targeted antioxidant and glycolysis inhibition: synergistic therapy in hepatocellular carcinoma. Anticancer Drugs *24(9)*: 881-888, 2013. PMID: 23872912. DOI: 10.1097/CAD.0b013e32836442c6

65 Millard M, Gallagher JD, Olenyuk BZ and Neamati N: A selective mitochondrial-targeted chlorambucil with remarkable cytotoxicity in breast and pancreatic cancers. J Med Chem *56(22)*: 9170-9179, 2013. PMID: 24147900. DOI: 10.1021/jm4012438

66 Singh G and Moorehead R: Mitochondria as a target for combination cancer-chemotherapy. Int J Oncol *1(7)*: 825-829, 1992. PMID: 21584623.

67 Hoye AT, Davoren JE, Wipf P, Fink MP and Kagan VE: Targeting mitochondria. Acc Chem Res *41(1)*: 87-97, 2008. PMID: 18193822. DOI: 10.1021/ar700135m

68 Skvortsov DA, Emashova SK, Kalinina MA and Dontsova OA: Cyanine mitochondrial dye with slightly selective cytotoxicity against A549 cancerous cells. Arch Pharm (Weinheim) *354(3)*: e2000281, 2021. PMID: 33245149. DOI: 10.1002/ardp.202000281

69 Starenki D and Park JI: Mitochondria-targeted nitroxide, Mito-CP, suppresses medullary thyroid carcinoma cell survival *in vitro* and *in vivo*. J Clin Endocrinol Metab *98(4)*: 1529-1540, 2013. PMID: 23509102. DOI: 10.1210/jc.2012-3671

70 Mazzio EA and Soliman KF: Effects of enhancing mitochondrial oxidative phosphorylation with reducing equivalents and ubiquinone on 1-methyl-4-phenylpyridinium toxicity and complex I-IV damage in neuroblastoma cells. Biochem Pharmacol *67(6)*: 1167-1184, 2004. PMID: 15006552. DOI: 10.1016/j.bcp.2003.11.016

71 Desai VG, Feuers RJ, Hart RW and Ali SF: MPP(+)-induced neurotoxicity in mouse is age-dependent: evidenced by the selective inhibition of complexes of electron transport. Brain Res *715(1-2)*: 1-8, 1996. PMID: 8739616. DOI: 10.1016/0006-8993(95)01255-9

72 Garofalo T, Ferri A, Sorice M, Azmoon P, Grasso M, Mattei V, Capozzi A, Manganelli V and Misasi R: Neuroglobin overexpression plays a pivotal role in neuroprotection through mitochondrial raft-like microdomains in neuroblastoma SK-N-BE2 cells. Mol Cell Neurosci *88*: 167-176, 2018. PMID: 29378245. DOI: 10.1016/j.mcn.2018.01.007

73 Rubio-Osornio M, Orozco-Ibarra M, Díaz-Ruiz A, Brambila E, Boll MC, Monroy-Noyola A, Guevara J, Montes S and Ríos C: Copper sulfate pretreatment prevents mitochondrial electron transport chain damage and apoptosis against MPP^+-induced neurotoxicity. Chem Biol Interact *271*: 1-8, 2017. PMID: 28442376. DOI: 10.1016/j.cbi.2017.04.016

74 Sablin SO, Krueger MJ, Yankovskaya VL, Tkachenko SE, Razdolsky AN, Bachurin SO, Ramsay RR and Singer TP: Inhibition of NADH oxidation by 1-methyl-4-phenylpyridinium analogs as the basis for the prediction of the inhibitory potency of novel compounds. J Biochem Toxicol *11(1)*: 33-43, 1996. PMID: 8806050. DOI: 10.1002/(SICI)1522-7146(1996)11:1<33::AID-JBT5>3.0.CO;2-W

75 Annepu J and Ravindranath V: 1-Methyl-4-phenyl-1,2,3,6-tetrahydropyridine-induced complex I inhibition is reversed by disulfide reductant, dithiothreitol in mouse brain. Neurosci Lett *289(3)*: 209-212, 2000. PMID: 10961666. DOI: 10.1016/s0304-3940(00)01300-8

76 Choi WS, Kruse SE, Palmiter RD and Xia Z: Mitochondrial complex I inhibition is not required for dopaminergic neuron death induced by rotenone, MPP+, or paraquat. Proc Natl Acad Sci USA *105(39)*: 15136-15141, 2008. PMID: 18812510. DOI: 10.1073/pnas.0807581105

77 Duz MB and Karatas OF: Expression profile of stem cell markers and ABC transporters in 5-fluorouracil resistant Hep-2 cells. Mol Biol Rep *47(7)*: 5431-5438, 2020. PMID: 32627138. DOI: 10.1007/s11033-020-05633-x

78 Kim J and Cheong JH: Role of mitochondria-cytoskeleton interactions in the regulation of mitochondrial structure and function in cancer stem cells. Cells *9(7)*, 2020. PMID: 32674438. DOI: 10.3390/cells9071691

79 Rodrigues T and Ferraz LS: Therapeutic potential of targeting mitochondrial dynamics in cancer. Biochem Pharmacol *182*: 114282, 2020. PMID: 33058754. DOI: 10.1016/j.bcp.2020.114282

80 Wang Z and Dong C: Gluconeogenesis in cancer: Function and regulation of PEPCK, FBPase, and G6Pase. Trends Cancer *5(1)*: 30-45, 2019. PMID: 30616754. DOI: 10.1016/j.trecan.2018.11.003

81 Moffett JR, Puthillathu N, Vengilote R, Jaworski DM and Namboodiri AM: Acetate revisited: A key biomolecule at the nexus of metabolism, epigenetics and oncogenesis-part 1: acetyl-CoA, acetogenesis and acyl-coa short-chain synthetases. Front Physiol *11*: 580167, 2020. PMID: 33281616. DOI: 10.3389/fphys.2020.580167

82 Martínez-Reyes I and Chandel NS: Acetyl-CoA-directed gene transcription in cancer cells. Genes Dev *32(7-8)*: 463-465, 2018. PMID: 29692354. DOI: 10.1101/gad.315168.118

83 Jha V, Galati S, Volpi V, Ciccone L, Minutolo F, Rizzolio F, Granchi C, Poli G and Tuccinardi T: Discovery of a new ATP-citrate lyase (ACLY) inhibitor identified by a pharmacophore-based virtual screening study. J Biomol Struct Dyn: 1-9, 2020. PMID: 32448086. DOI: 10.1080/07391102.2020.1773314

84 Icard P, Wu Z, Fournel L, Coquerel A, Lincet H and Alifano M: ATP citrate lyase: A central metabolic enzyme in cancer. Cancer Lett *471*: 125-134, 2020. PMID: 31830561. DOI: 10.1016/j.canlet.2019.12.010

85 Ciregia F: Mitochondria lysine acetylation and phenotypic control. Adv Exp Med Biol *1158*: 59-70, 2019. PMID: 31452135. DOI: 10.1007/978-981-13-8367-0_4

86 Ignatova VV, Jansen PWTC, Baltissen MP, Vermeulen M and Schneider R: The interactome of a family of potential methyltransferases in HeLa cells. Sci Rep *9(1)*: 6584, 2019. PMID: 31036863. DOI: 10.1038/s41598-019-43010-2

87 Arcidiacono OA, Krejčí J and Bártová E: The distinct function and localization of METTL3/METTL14 and METTL16 enzymes in cardiomyocytes. Int J Mol Sci *21(21)*: 2020. PMID: 33143367. DOI: 10.3390/ijms21218139

88 Soldner F, Weller M, Haid S, Beinroth S, Miller SW, Wüllner U, Davis RE, Dichgans J, Klockgether T and Schulz JB: MPP+ inhibits proliferation of PC12 cells by a p21(WAF1/Cip1)-dependent pathway and induces cell death in cells lacking p21(WAF1/Cip1). Exp Cell Res *250(1)*: 75-85, 1999. PMID: 10388522. DOI: 10.1006/excr.1999.4504

89 Amo T, Oji Y, Saiki S and Hattori N: Metabolomic analysis revealed mitochondrial dysfunction and aberrant choline metabolism in MPP^+-exposed SH-SY5Y cells. Biochem Biophys Res Commun *519(3)*: 540-546, 2019. PMID: 31537380. DOI: 10.1016/j.bbrc.2019.09.031

90 Badisa RB, Darling-Reed SF and Soliman KF: The protective role of D-glucose against 1-methyl-4-phenylpyridinium ion (MPP+): induced mitochondrial dysfunction in C6 astroglial cells. Neurochem Res *35(9)*: 1413-1421, 2010. PMID: 20508987. DOI: 10.1007/s11064-010-0200-9

91 Wu T, Li Y, Liu B, Zhang S, Wu L, Zhu X and Chen Q: Expression of ferritin light chain (FTL) is elevated in glioblastoma, and FTL Silencing inhibits glioblastoma cell proliferation *via* the GADD45/JNK pathway. PLoS One *11(2)*: e0149361, 2016. PMID: 26871431. DOI: 10.1371/journal.pone.0149361

92 Neuteboom ST, Karjian PL, Boyer CR, Beryt M, Pegram M, Wahl GM and Shepard HM: Inhibition of cell growth by NB1011 requires high thymidylate synthase levels and correlates with p53, p21, bax, and GADD45 induction. Mol Cancer Ther *1(6)*: 377-384, 2002. PMID: 12477050

93 Huang WS, Kuo YH, Kuo HC, Hsieh MC, Huang CY, Lee KC, Lee KF, Shen CH, Tung SY and Teng CC: CIL-102-induced cell cycle arrest and apoptosis in colorectal cancer cells *via* upregulation of p21 and GADD45. PLoS One *12(1)*: e0168989, 2017. PMID: 28068431. DOI: 10.1371/journal.pone.0168989

94 Schweich LC, Oliveira EJT, Pesarini JR, Hermeto LC, Camassola M, Nardi NB, Brochado TMM, Antoniolli-Silva ACMB and Oliveira RJ: All-trans retinoic acid induces mitochondria-mediated apoptosis of human adipose-derived stem cells and affects the balance of the adipogenic differentiation. Biomed Pharmacother *96*: 1267-1274, 2017. PMID: 29239820. DOI: 10.1016/j.biopha.2017.11.087

Received February 15, 2021
Revised March 15, 2021
Accepted April 6, 2021